Possible atmospheric CO_2 extremes of the Middle Cretaceous (late Albian–Turonian)

Karen L. Bice and Richard D. Norris[1]

Department of Geology and Geophysics, Woods Hole Oceanographic Institution, Woods Hole, Massachusetts, USA

[1] Atmospheric carbon dioxide (CO_2) estimates for the Middle Cretaceous (MK) have a range of >4000 ppm, which presents considerable uncertainty in understanding the possible causes of warmth for this interval. This paper examines the problem of MK greenhouse forcing from an inverse perspective: we estimate upper ocean water temperatures from oxygen isotope measurements of well-preserved late Albian–Turonian planktonic foraminifera and compare these against temperatures predicted by general circulation model (GCM) experiments with CO_2 concentrations of 500–7500 ppm. At least 4500 ppm CO_2 is required to match maximum temperatures inferred from well-preserved planktonic foraminifera. Approximately 900 ppm CO_2 produces a good match between the model and the minimum temperature estimates for the MK. An ocean model forced by these two extremes in surface conditions brackets nearly all available bottom water temperature estimates for this interval. The climate model results support nearly the entire range of MK CO_2 estimates from proxy data. The ocean model suggests possible MK oceanographic changes from deep water formation in the high latitude region of one hemisphere to the other hemisphere in response to changes in atmospheric temperatures and hydrologic cycle strength. We suggest that, rather than contradicting one another, the various proxy CO_2 techniques (especially those with high temporal resolution) may capture true variability in CO_2 concentrations and that MK CO_2 could have varied by several thousand ppm through this interval. *INDEX TERMS:* 3344 Meteorology and Atmospheric Dynamics: Paleoclimatology; 3374 Meteorology and Atmospheric Dynamics: Tropical meteorology; 4806 Oceanography: Biological and Chemical: Carbon cycling; 1836 Hydrology: Hydrologic budget (1655); *KEYWORDS:* CO_2, Middle Cretaceous, greenhouse, planktonic foraminifera, climate model

1. Introduction

[2] The Middle Cretaceous (MK) (∼105–89 Ma) encompasses one of the warmest climate intervals of the Phanerozoic [*Veizer et al.*, 2000]. High latitude continents exhibited cool to warm temperate climates [*Askin and Spicer*, 1995; *Herman and Spicer*, 1996; *Tarduno et al.*, 1998]. Recent oxygen isotope data indicate that tropical sea surface temperatures (SSTs) in the late Albian through Turonian interval may have been as high as 35°C [*Norris et al.*, 2002; *Wilson et al.*, 2002] and high latitude SSTs were 20°C or higher [*Huber et al.*, 1995]. Available bottom water temperature estimates for paleodepths greater than 1000 m range between 11°C and 19°C [*Huber et al.*, 1999, 2002].

[3] The MK is held up as an analog for future climates, if greenhouse gas-induced warming continues [*Crowley*, 1996]. However, reconstructions of atmospheric carbon dioxide (CO_2) concentrations for the MK encompass a range of <900 to >4000 ppm volumetrically (Figure 1). The upper bound to this range comes from fossil leaf

stomatal index (SI) measurements of Cenomanian and Turonian *Ginkgo* specimens from Siberia that yield CO_2 values of 4000–5500 ppm [*Retallack*, 2001]. At the bottom of the range, *Freeman and Hayes* [1992] provide estimates of 830–1100 ppm CO_2 based on the carbon isotopic composition of marine organic compounds in Cenomanian and Turonian sediments of the Western Interior Seaway and North Atlantic. Carbon cycle model estimates [*Berner and Kothavala*, 2001; *Wallmann*, 2001a] and soil carbonate proxy records [*Ekart et al.*, 1999] yield CO_2 estimates that fall between the fossil leaf and geochemical proxies. The wide range of paleo-CO_2 reconstructions, including estimates lower than or equal to the modern for the relatively warm early Cenozoic, has led to scrutiny of the CO_2–climate link [*Cowling*, 1999; *Flower*, 1999; *Crowley and Berner*, 2001] and critical review of the various proxy techniques [*Royer et al.*, 2001]. However, the question remains: Is the >4000 ppm range of estimates for the MK real, such that short-term variations (<1 Myr) in CO_2 have been captured by proxy methods with high temporal resolution (leaf stomata and marine organic $\delta^{13}C$), or does it result primarily from the widely varying precision and assumptions of the various methods used to reconstruct past atmospheric CO_2 concentrations? In either case, the range of published estimates presents considerable uncertainty in the magnitude of radiative gas forcing that can be

---

[1]Now at Scripps Institution of Oceanography, University of California, San Diego, La Jolla, California, USA.
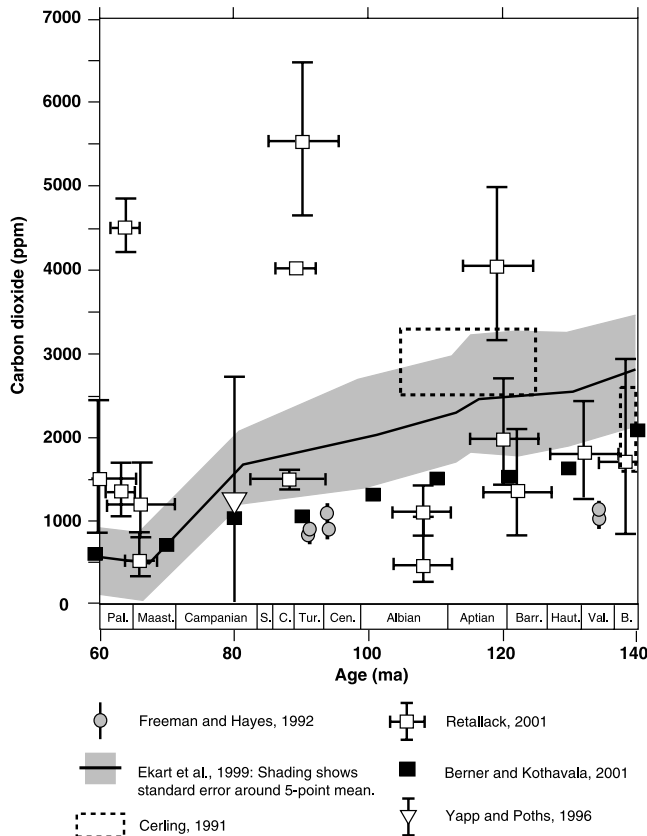
Figure 1. Compilation of atmospheric CO$_2$ concentration estimates for 60–140 Ma.

called upon to explain climate conditions inferred for this interval of extreme warmth.

[4] From the perspective of a simple global energy balance model, greenhouse warming ~12–36% greater than the modern is supported for the MK. Earth's effective radiating temperature (T_e) is a function of the solar flux (S) and albedo (A) according to the relationship:

$$\sigma T_e^4 = (S/4)(1 - A)$$

where σ is the Stefan–Boltzmann constant (5.67×10^{-8} W m^{-2} K^{-4}) and S today is approximately equal to 1365 W m^{-2}. Surface temperature (T_s) is in turn the sum of T_e and the warming due to radiative gases in the atmosphere (mainly H$_2$O, CO$_2$, and CH$_4$), known as the greenhouse effect. Earth's mean albedo today is ~30% and surface temperature is ~15°C, yielding a greenhouse effect of ~+33°C.

[5] Based on a simple linear model of main sequence stellar evolution, solar luminosity was ~1% lower at 100 Ma than today [*Gough*, 1981]. Albedo change between the MK and today involves competing effects: ice-free poles and extensive green vegetation coverage would have lowered surface albedo, while possible greater cloud cover in a warmer, wetter atmosphere [*Manabe*, 1996] would have had a positive feedback on albedo. With a 1% reduction in solar luminosity and the modern greenhouse effect, the MK Earth Mcould have attained the same mean surface temperature as

today, if albedo was as little as 0.5% less than the modern. However, climate model simulations that produce reasonably good matches to MK temperature estimates indicate global mean surface temperatures of 21–28°C [*Poulsen*, 1999; this study]. To attain these temperatures without greater greenhouse warming, an albedo decrease of 8–17% would be required, considerably more than the 2–4% reduction calculated for MK land/sea distribution, ice-free poles, and global green vegetation coverage [this study]. If proxy estimates of T_s and A are realistic, a greenhouse effect 4–12°C greater than the modern is supported for the MK.

[6] This additional warming can be accomplished by some combination of increased atmospheric water vapor, CO$_2$, and methane. An increase in atmospheric water vapor concentration is expected as a positive feedback to warming induced by any increase in greenhouse gases other than water vapor. In addition, warmer, wetter climates in the past 500 kyr have exhibited atmospheric methane increases along with CO$_2$, so it is reasonable to expect that the warmer, wetter MK may have had atmospheric methane concentrations higher than the modern (~1.65 ppm), but how much higher is entirely unconstrained.

[7] General circulation models (GCMs) represent perhaps the most sophisticated method for establishing plausible atmospheric boundary conditions consistent with paleoclimate data. GCMs have a number of fundamental advantages over less expensive, one-dimensional radiative-convective models [e.g., *Ramanathan et al.*, 1979; *Kiehl and Dickinson*, 1987]. The effect of land/sea distribution on surface temperature and supply of moisture to the atmosphere is readily incorporated in GCMs so that relative humidity can evolve in response to boundary conditions, and the model includes the snow/ice–albedo feedback, which can be important at lower polar temperature values [*Berner and Barron*, 1984]. Numerous MK GCM studies have specified CO$_2$ concentrations in the range 720–2040 ppm in order to produce reasonable matches to quantitative and semiquantitative continental and ocean climate reconstructions [*Barron et al.*, 1993b; *Price et al.*, 1998a; *Beerling et al.*, 1999; *Poulsen et al.*, 1999a, 1999b]. However, the role of reduced solar luminosity and the radiative forcing of possible increased atmospheric methane concentrations are parameters that have largely been neglected in previous MK studies.

[8] Note that, in the Cretaceous literature, atmospheric CO$_2$ concentrations are often expressed as multiples of the modern value. In model studies by Barron, Poulsen, and colleagues cited above, for example, the CO$_2$ concentrations used are expressed as multiples of the "present-day" value, where the present-day value was taken as 340 ppm, the approximate value for 1983. In 2002, Earth's global average CO$_2$ concentration is just above 370 ppm (data are available from the NOAA World Wide Web CMDL Data Archive server at http://www.cmdl.noaa.gov/). Because Earth's CO$_2$ is currently increasing so rapidly, we encourage the use of absolute values in climate model publications, or multiples of the canonical "preindustrial" value of 280 ppm.

[9] In the current study, we examine the question of plausible MK greenhouse effects using GCMs in order to identify CO$_2$ extremes consistent with the full range of

temperatures within the late Albian–Turonian interval. The data–model comparison incorporates newly available data from very well-preserved tropical and subtropical planktonic foraminifera that indicate SSTs 5–6°C warmer than the warmest modern temperatures at those latitudes [*Norris et al.*, 2002; *Wilson et al.*, 2002]. We vary atmospheric CO$_2$, CH$_4$, solar luminosity, and ocean heat transport parameters in an atmospheric GCM with a slab ocean. The output from selected atmospheric model experiments is used to force an ocean model. Our objective is to determine what atmospheric CO$_2$ concentrations simultaneously satisfy MK polar continental climate reconstructions, and upper ocean and ocean bottom temperature estimates. The approach taken is to define the model boundary conditions that result in zonal mean SSTs that bracket minimum and maximum isotopic paleotemperature estimates. By comparing model results with both minimum and maximum temperature estimates for this interval, we conclude that it is possible that the MK exhibited nearly the entire range of values of CO$_2$ indicated by the proxy records.

2. Water Temperature Calculations

2.1. Upper Ocean Temperatures

[10] Oxygen isotope data for planktonic foraminifera were compiled from late Albian through Turonian deep sea drill sites. Of these sites, data for all (DSDP Sites 305 and 551) or part (Albian in DSDP Site 327, Turonian in DSDP Site 463, and ODP Site 1050) of five sites were excluded owing to poor to moderate preservation. Data from foraminifera known to be thermocline dwelling species (*Rotalipora* and *Dicarinella*) were also excluded. For each remaining locality and for each species, the minimum and maximum δ^{18}O values are shown in Table 1 and in Figure 3a. Note that the biostratigraphic zone ages in Tables 1 and 2 are those reported in the published sources and these do not use one consistent zonation scheme. There can be large age differences among samples identified in the literature as "late Albian," for example: samples from nannofossil zone NC9B at DSDP Site 392 are ~5 million years older than the oldest Albian samples from ODP Site 1050 (B. Huber, personal communication, 2002). This illustrates the problem associated with restricting a study such as ours to more narrowly defined Cretaceous time intervals: too few data would be available to constrain ocean temperature gradients. Even in our compilation of a broad interval of the MK, data are not widely distributed among ocean basins: Six of the 9 sites in the compilation of planktonics are located in the Atlantic basins, one is in the southern Indian Ocean, and two are central Pacific sites (Figure 2). Of the five sites in the North Atlantic basin, four are in the western subtropical Blake Nose/Blake Plateau area.

[11] Upper ocean paleotemperatures were calculated using the equation of *Erez and Luz* [1983], which has an estimated uncertainty of ~±1.8°C [*Bice et al.*, 2000]. To convert water δ^{18}O values from Standard Mean Ocean Water (SMOW) to the Pee Dee Belemnite (PDB) scale, −0.27‰ was used [*Hut*, 1987]. An average ocean water δ^{18}O (δ_w) value of −1.0‰ (SMOW) was assumed [*Shackleton and Kennett*, 1975] to adjust for the absence of large ice

sheets in the MK. For planktonic calculations, an additional adjustment was made to local upper ocean water δ^{18}O based on a fit to the modern latitude–δ_w relationship [*Zachos et al.*, 1994]. The δ_w values used in planktonic calculations are shown in Figure 3a. Although the resulting paleotemperatures are plotted in Figure 3b as a function of paleolatitude and compared against zonal mean SSTs simulated by the atmospheric climate model, we stress that individual calculations should not be thought of as equal to zonal mean temperatures for their respective time periods. Ocean and atmospheric circulation produce important water temperature differences along lines of latitude. However, so few data exist for any one time period (and, indeed, for the entire MK interval chosen here) that it is currently impossible to define longitudinal variability in actual MK upper ocean temperatures from the existing data. We consider the comparison of the compiled estimates against zonally averaged fields from the model to be adequate for a first approximation of the model–data fit.

[12] It is apparent from Figure 3 that most Turonian data from Site 511 planktonic foraminifera are anomalously light for 60°S latitude. Although tropical and benthic isotopic data [*Huber et al.*, 1995; *Wilson et al.*, 2002] also support the idea that the Turonian was the warmest interval of the MK, the extreme high latitude warmth (as warm as ~31°C at 60°S latitude) implied by the Site 511 values is currently unsupported by any other data, in either hemisphere for any time in known geologic history. We return to the Site 511 Turonian data in the discussion below (section 5.1), but, because these data result in temperature estimates that are currently uncorroborated in any way, we prefer to set them aside for now as problematic.

2.2. Ocean Bottom Temperatures

[13] Generally, so few MK benthic foraminiferal isotope data are available that we have compiled either all measurements on well-preserved specimens (Sites 144, 258, 392, and 511) or, where more than 2–3 measurements are reported, the minimum and maximum value for each species within each informal stage subdivision, late Albian through late Turonian (Sites 1050 and 1052) (Table 2). Temperatures were again calculated using the equation of *Erez and Luz* [1983], except for three measurements by *Norris and Wilson* [1998] on aragonitic benthic species. In that case, paleotemperatures were calculated using equation (1) of *Grossman and Ku* [1986] for aragonitic carbonate. For benthic temperature calculations, we assume a δ_w value of −1.0‰ (SMOW), but note that bottom water δ^{18}O can also deviate from the mean ocean value. Bottom water temperature uncertainty estimates are therefore made using the standard deviation of modern values in δ_w in the depth ranges of the MK sites. This allows for some consideration of the large uncertainty in the appropriate δ_w values at the shallow paleodepths of several of the MK sites and provides a first-order uncertainty estimate for δ_w at deeper sites. The standard deviation of *GEOSECS* [1987] δ_w values was calculated for 2 depth ranges corresponding to the paleodepths of the MK sites: 100–600 and 1500–2500 m. The resulting σ values are 0.33 and 0.14, respectively. Uncertainties in bottom water paleotemperatures for these depths

Table 1. Oxygen Isotope Values From Planktonic Foraminifera

Species	Age/Biostratigraphic Zone	mbsf	δ^{18}O	Source
Site 144, Demerara Rise, North Atlantic, 5°N				
Globigerinoides bentonensis	latest Cenomanian, IC 50	215.19	−3.437	*Sellwood et al.* [1994],
Globigerinoides bentonensis	latest Cenomanian, IC 50	216.73	−3.760	*Norris et al.* [2002],
Hedbergella amabalis	middle to late Turonian, UC 9a	181.15	−3.558	*Wilson et al.* [2002]
Hedbergella amabalis	middle to late Turonian, UC 9a	190.05	−4.397	
Hedbergella delrioensis	latest Cenomanian, IC 50	216.62	−3.553	
Hedbergella delrioensis	middle to late Turonian, UC 9a	190.42	−4.356	
Hedbergella sp.	late Cenomanian to early Turonian	not given	−3.24	
Heterohelix globulosa	middle to late Turonian, UC 9a	181.15	−3.688	
Heterohelix globulosa	middle to late Turonian, UC 9a	190.05	−4.345	
Heterohelix moremani	middle to late Turonian, UC 9a	189.75	−3.662	
Heterohelix moremani	middle to late Turonian, UC 9a	190.05	−4.509	
Whiteinella sp.	latest Cenomanian, IC 50	217.35	−3.659	
Site 171, Horizon Guyot, East Central Pacific, 15°S				
"Planktonic assemblage"	early Turonian, *M. hagni*	315–325	−3.40	*Douglas and Savin* [1973]
"Planktonic assemblage"	late Turonian, *M. helvetica*	306–315	−4.03	
Site 258, Naturaliste Plateau, Southern Indian Ocean, 62°S				
Hedbergella delrioensis	late Cenomanian, *G. obliq.*	263.83	−1.85	*Huber et al.* [1995]
Site 392, Blake Nose, North Atlantic, 30°N				
Hedbergella spp.	late Albian, NC 9B	69.28	−1.27	*Fassell and Bralower* [1999]
Hedbergella spp.	late Albian, NC 9B	66.66	−2.37	
Site 463, mid-Pacific Mountains, East Central Pacific, 17°S				
Hedbergella delrioensis	middle to late Cenomanian, *R. cush.*	382.83	−2.492	*Price et al.* [1998b]
Hedbergella delrioensis	middle to late Cenomanian, *R. cush.*	382.83	−3.097	
Site 511, Falkland Plateau, South Atlantic, 60°S				
Archaeoglob bosquensis	Turonian, *K. magni.*	410.18	−3.86	*Huber et al.* [1995]
Archaeoglob bosquensis	Turonian, *K. magni.*	411.68	−4.35	
Globotruncana bulloides	Turonian, *K. magni.*	408.73	−3.53	
Globotruncana bulloides	Turonian, *K. magni.*	411.68	−4.39	
Hedbergella spp.	late Albian, *E. turr.*	435.76	−0.71	
Hedbergella spp.	late Cenomanian	429.24	−1.42	
Whiteinella baltica	Turonian, *K. magni.*	413.74	−2.31	
Whiteinella baltica	Turonian, *K. magni.*	411.68	−3.34	
Whiteinella brittonensis	late Cenomanian	429.24	−1.91	
Site 627, Blake Plateau, North Atlantic, 25°N				
"Mixed Planktonics"	early middle Cenomanian	not given	−2.32	*Sellwood et al.* [1994]
"Mixed Planktonics"	early middle Cenomanian	not given	−2.43	
Site 1050, Blake Nose, North Atlantic, 30°N				
Briticinella breggiensis	late Albian, *R. appenninica*	567.80	−2.211	*Huber et al.* [1999, 2002]
Briticinella breggiensis	early Cenomanian, *R. glob.*	529.08	−3.714	
Costellagerina libyca	late Albian, *R. appenninica*	552.13	−2.385	
Costellagerina libyca	late Albian, *R. appenninica*	553.73	−3.418	
Globigerinoides bentonensis	late Cenomanian, *R. cush.*	510.13	−2.370	
Globigerinoides bentonensis	late Albian, *R. ticinensis*	600.20	−2.655	
Hedbergella delrioensis	middle Cenomanian, *R. reicheli*	519.44	−1.574	
Hedbergella delrioensis	middle Cenomanian, *R. reicheli*	521.60	−3.270	
Hedbergella simplex	early Cenomanian, *R. glob.*	531.29	−1.664	
Hedbergella simplex	late Albian, *R. appenninica*	561.79	−2.435	
Heterohelix moremani	middle Cenomanian, *R. reicheli*	519.44	−1.248	
Heterohelix moremani	early Cenomanian, *R. glob.*	531.91	−2.710	
Ticinella primula	late Albian, *R. ticinensis*	603.21	−2.495	
Ticinella primula	late Albian, *R. ticinensis*	600.20	−3.692	
Whiteinella archaeocreta	late Cenomanian, *R. cush.*	505.99	−2.098	
Whiteinella archaeocreta	late Cenomanian, *R. cush.*	509.25	−3.309	
Whiteinella baltica	late Cenomanian, *R. cush.*	501.12	−1.621	
Whiteinella baltica	late Cenomanian, *R. cush.*	508.24	−2.364	
Whiteinella brittonensis	late Cenomanian, *R. cush.*	501.40	−2.154	
Whiteinella brittonensis	early Cenomanian, *R. glob.*	523.67	−2.756	
Site 1052, Blake Nose, North Atlantic, 30°N				
Briticinella breggiensis	late Albian, *R. ticinensis*	532.59	−2.25	*Norris and Wilson* [1998],
Briticinella breggiensis	late Albian, *R. appenninica*	529.05	−3.74	*Wilson and Norris* [2001]
Costellagerina libyca	late Albian, *R. appenninica*	513.28	−3.69	
Costellagerina libyca	late Albian, *R. appenninica*	512.30	−1.93	

Table 1. (continued)

Species	Age/Biostratigraphic Zone	mbsf	δ^{18}O	Source
Planomalina buxtorfi	late Albian, *R. ticinensis*	532.59	−1.86	
Planomalina buxtorfi	late Albian, *R. appenninica*	513.51	−3.20	
Planomalina praebuxtorfi	late Albian, *R. ticinensis*	545.89	−2.48	
Planomalina praebuxtorfi	late Albian, *R. ticinensis*	533.88	−3.73	
Ticinella primula	late Albian, *R. ticinensis*	627.41	−2.54	
Ticinella primula	late Albian, *R. ticinensis*	630.15	−3.96	
Ticinella raynaudi	late Albian, *R. ticinensis*	637.17	−2.32	

Table 2. Oxygen Isotope Values From Benthic Foraminifera

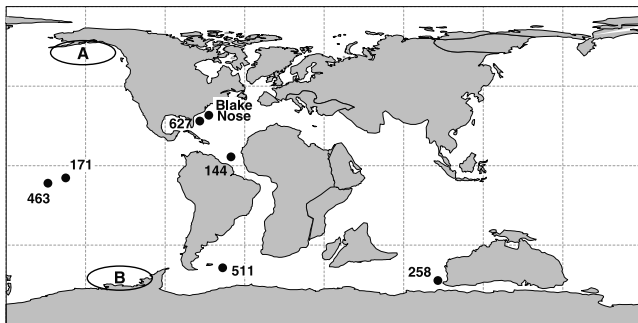| Species	Age/Biostratigraphic Zone	mbsf	δ^{18}O	Source
	Site 144, Demerara Rise, North Atlantic, Paleodepth 1700 m			
benthic sp.	middle to late Turonian, UC 9a	189.75	−0.600	*Wilson et al.* [2002]
benthic sp.	middle to late Turonian, UC 9a	189.75	−0.837	
	Site 258, Naturaliste Plateau, Southern Indian Ocean, Paleodepth 1500 m			
Angulogavelinella sp.	late Cenomanian, *G. obliq.*	263.83	−0.80	*Huber et al.* [1995]
	Site 392, Blake Nose, North Atlantic, Paleodepth 1800 m			
Gavelinella spp. (rounded)	late Albian, NC 9B	69.91	−0.06	*Fassell and Bralower* [1999]
Gavelinella spp. (rounded)	late Albian, NC 9B	66.66	−0.96	
	Site 511, Falkland Plateau, South Atlantic, Paleodepth 100−400 m			
Gavelinella sp.	late Cenomanian	429.24	−0.38	*Huber et al.* [1995],
Gavelinella spp. (pl-con.)	late Albian, *E. turr.*	432.77	−0.36	*Fassell and Bralower* [1999]
Gavelinella spp. (pl-con.)	late Albian, *E. turr.*	432.77	−0.40	
Gavelinella spp. (rounded)	late Albian, *A. albianus*	437.20	−0.12	
Gavelinella spp. (rounded)	late Albian, *E. turr.*	434.53	−0.66	
Gyroidina globosa	late Albian, *E. turr.*	430.74	−0.33	
Gyroidina globosa	late Albian, *E. turr.*	435.76	−0.24	
"mixed benthics"	Turonian, *K. magni.*	407.23	−1.46	
"mixed benthics"	Turonian, *K. magni.*	413.74	−1.53	
	Site 1050, Blake Nose, North Atlantic, Paleodepth 1500 m			
Berthelina sp.	late Cenomanian, *R. cush.*	510.26	−0.462	*Huber et al.* [1999, 2002]
Berthelina sp.	middle Cenomanian, *R. reicheli*	521.89	−0.762	
Berthelina sp.	early Cenomanian, *R. glob.*	523.71	−0.410	
Berthelina sp.	early Cenomanian, *R. glob.*	532.45	−0.832	
Berthelina sp.	late Albian, *R. appenninica*	563.84	0.150	
Berthelina sp.	late Albian, *R. appenninica*	571.20	−0.946	
Berthelina sp.	late Albian, *R. ticinensis*	597.21	−0.328	
Berthelina sp.	late Albian, *R. ticinensis*	606.00	−1.540	
Cibicides sp.	late Cenomanian, *R. cush.*	510.21	−0.716	
Gavelinella sp.	Cenomanian−Turonian OAE2	500.95	−1.075	
Gavelinella sp.	Cenomanian−Turonian OAE2	500.91	−1.613	
Gavelinella sp.	late Cenomanian, *R. cush.*	501.01	−0.812	
Gavelinella sp.	late Cenomanian, *R. cush.*	501.12	−1.184	
Gavelinella sp.	middle Cenomanian, *R. reicheli*	521.60	0.069	
Gavelinella sp.	middle Cenomanian, *R. reicheli*	521.60	0.069	
Gavelinella sp.	early Cenomanian, *R. glob.*	523.71	−0.381	
Gavelinella sp.	early Cenomanian, *R. glob.*	532.45	−0.811	
Gavelinella sp.	late Albian, *R. appenninica*	552.13	−0.518	
Gavelinella sp.	late Albian, *R. appenninica*	560.35	−0.861	
Gavelinella sp.	late Albian, *R. ticinensis*	604.69	−0.593	
Gyroidina globosa	late Cenomanian, *R. cush.*	505.33	−0.814	
Gyroidina globosa	late Cenomanian, *R. cush.*	508.75	−0.596	
Gyroidina globosa	late Albian, *R. appenninica*	553.73	−0.619	
Nuttalides sp.	early Cenomanian, *R. glob.*	541.03	0.070	
"mixed benthics"	middle Cenomanian, *R. reicheli*	519.44	0.023	
"mixed benthics"	early Cenomanian, *R. glob.*	522.90	−0.504	
"mixed benthics"	early Cenomanian, *R. glob.*	543.36	−0.749	
	Site 1052, Blake Nose, North Atlantic, Paleodepth 500 m			
Aragonitic species	early Cenomanian	483.3	−1.127	*Norris and Wilson* [1998]
Aragonitic species	late Albian, *R. ticinensis*	571.5	−0.595	
Aragonitic species	late Albian, *R. ticinensis*	617.4	−0.336	
Gyroidinoides	late Albian to early Cenomanian (100 measurements)		−0.72 to 2.44	P. A. Wilson (unpublished data)

Figure 2. Paleogeographic reconstruction [after *Barron*, 1987] for the Cenomanian showing locations of sites discussed in the study. Ovals indicate regions of dominant deep water formation in the ocean model given (a) cooler (900 ppm CO$_2$, QFACT = 5) and (b) warmer (4500 ppm CO$_2$, QFACT = 4) boundary conditions. Sites DSDP 392, ODP 1050, and ODP 1052 are located on Blake Nose.

calculated using $\delta_w = -1.0 \pm 2\sigma$ ‰ (SMOW) in the Erez and Luz equation are $\pm 3.0°C$ and $\pm 1.3°C$, respectively.

[14] For the purpose of model–data comparison, we use published paleodepth estimates where possible in Table 2. Following the study of *Norris et al.* [1998], we estimate minimum paleodepths for Blake Nose at 500 m for Site 1052, 1500 m for Site 1050, and 1800 m for DSDP Site 392 (ODP Site 1049). These estimates assume that the Aptian–Albian reef system identified on seismic data from the area was at sea level in the Albian and the various drill sites were at greater water depths to the east of that reef. The top of the Albian–Cenomanian sequence in ODP Site 1052 is ∼500 m deeper than the reef crest, suggesting a paleodepth of at least 500 m, while Sites 1050 and 392 are 1000 and 1300 m, respectively, deeper than 1052. Because these sites are underlain by >8 km of Jurassic–Cretaceous limestone, it is unlikely that the sites have subsided very much relative to each other since the Albian.

3. Model Boundary Conditions

3.1. Atmospheric Model Experiments

[15] The atmospheric model used is the GENESIS v. 2.0 global climate model [*Thompson and Pollard*, 1997]. GENESIS is a T31 spectral atmospheric GCM coupled to a nondynamical 50 m slab mixed-layer ocean model (below) and multilayer snow, ice, and soil modules. Geography consists of a 2° resolution reconstruction of middle to late Cenomanian (∼95 Ma) paleogeography based on the Cenomanian continental positions of *Barron* [1987] and qualitative topographic reconstruction of *Scotese and Golonka* [1992]. A globally uniform, mixed vegetation was specified everywhere on the continents. Earth orbital parameters were held constant at modern values. Solar luminosity was set at either the modern value (1365 W m^{-2}) or 99% of the modern (1351.4 W m^{-2}), to adjust for lower MK solar luminosity [*Gough*, 1981]. Atmospheric methane was set at the approximate modern value of 1.65 ppm, except in one sensitivity experiment where 16.5 ppm CH$_4$ was used. (The methane test performed here is meant simply as a first-order model

sensitivity test.) We varied atmospheric CO$_2$ concentration between 500 and 7500 ppm in a series of sensitivity tests designed to produce a reasonable match in annual mean zonal ocean surface temperature and upper ocean paleotemperatures calculated from planktonic foraminifera.

[16] Producing a fit to isotopic paleotemperatures also requires tuning the ocean heat transport parameter in the model. Previous Cretaceous studies using GENESIS [*Barron et al.*, 1993a, 1993b, 1995; *Deconto et al.*, 1999, 2000; *Poulsen et al.*, 1999a] have shown that increasing CO$_2$ alone fails to reproduce the polar warmth and reduced surface temperature gradient inferred for the Cretaceous and that a tuning is also required in the parameterization of ocean heat transport. In GENESIS, the ocean is represented by a nondynamical, 50 m thermodynamic slab that captures the seasonal heat capacity of the mixed layer. Oceanic heat transport is parameterized as linear diffusion down the local gradient in slab ocean temperature according
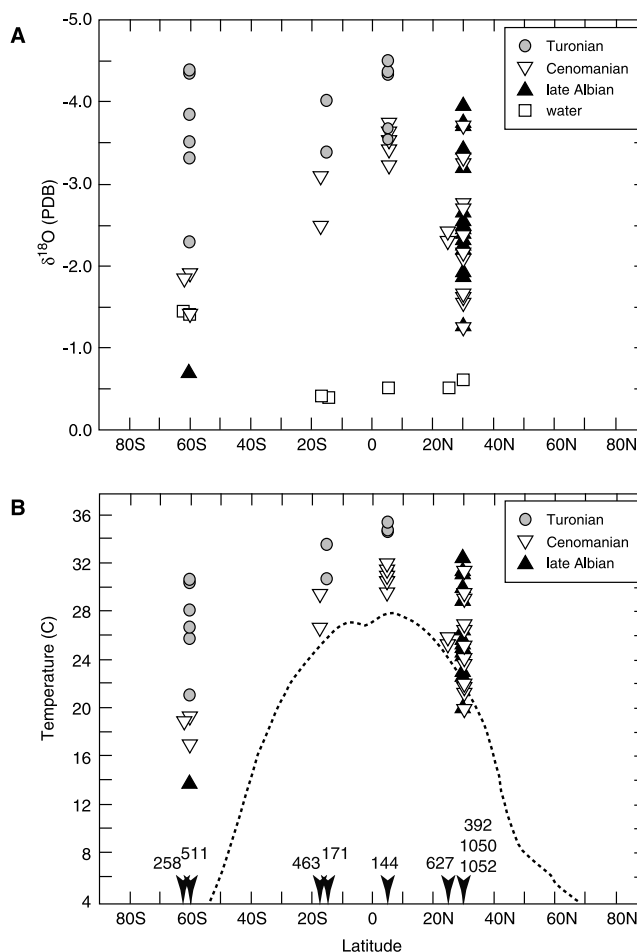

Figure 3. (a) Carbonate $\delta^{18}O$ values for planktonic foraminifera, plotted as a function of paleolatitude. Values are given in Table 1. Open squares indicate the water $\delta^{18}O$ value used in the isotopic paleotemperature equation. (b) Upper ocean temperatures calculated from the carbonate values in panel (a). The dashed line indicates the zonal mean of modern SSTs. Site numbers are indicated along the bottom of the lower panel.

to a diffusion coefficient depending on zonal land/ocean fraction and latitude.

[17] A multiplicative factor (herein referred to as QFACT) can be applied to the diffusion coefficient in order to increase or decrease the parameterized magnitude of the oceanic heat transport. QFACT = 1 indicates no increase/decrease in the coefficient from that determined by the local temperature gradient and land/ocean fraction. Producing a match between GENESIS temperatures and those inferred from Cretaceous isotope data requires multiplying the slab ocean diffusion coefficient by QFACT > 1. QFACT values of from 2 to 4 have been used in previous GENESIS experiments to obtain reasonable matches to Cretaceous data (references above). We tested QFACT values of 2–25 and found that a value of 4 or 5 is needed to match gradients defined by the extremes in temperature inferred from the compiled δ^{18}O data (excluding, for now, the problematic Site 511 Turonian data). Values of 1 or 2 yield SST profiles that approximate the maximum pole-to-equator temperature gradient allowable within the compiled data.

[18] How does the magnitude of QFACT correspond to the magnitude of the model's implied ocean heat transport? Estimates of modern maximum ocean heat transport vary between 1.5 and 3.0 × 10^{15} W in the Northern Hemisphere and 0.5 and 1.5 × 10^{15} W in the Southern Hemisphere [*Ganachaud and Wunsch*, 2000; *Garnier et al.*, 2000; *Trenberth and Caron*, 2001]. For the MK paleogeography, QFACT values of 4–5 result in implied maximum ocean heat transport values (calculated from the annual net heat flux into the ocean surface at each latitude) that are within the range of modern estimates in the Northern Hemisphere (2.0 × 10^{15} W) and approximately 2 times greater than maximum modern estimates in the Southern Hemisphere (2.75 × 10^{15} W). This illustrates the important point that a multiplicative factor of N in the GENESIS ocean heat parameter does not equal a N-fold increase over modern ocean heat transport. How QFACT scales to modern transport is dependent on the predicted local temperature gradient. Because of the negative feedback between QFACT and the ocean temperature gradient, the relationship between QFACT and implied ocean heat transport is nonlinear; the greatest increases in implied heat transport are obtained with lower values (2–3) of QFACT. As the target SST gradient decreases, exponentially larger QFACT values are required. The rate of increase in implied ocean heat transport with increasing QFACT slows dramatically above QFACT = 7.

3.2. Ocean Model Experiments

[19] Modern planktonic foraminifera live and add calcium carbonate over a range of depths within the upper ocean, so many species do not strictly record SST, but this is the only "ocean" temperature value that is predicted by the atmospheric model. The lack of a dynamical ocean in the atmospheric model also means that the temperature effects of boundary currents and upwelling are not included. Therefore, to better determine which CO$_2$ levels produce a plausible match to inferred paleoocean conditions, the GFDL Modular Ocean Model v. 2 (MOM2) was forced with output from selected GENESIS runs. MOM2 is a full global, three-dimensional, primitive equation ocean circulation model widely used in modern and paleoocean experi-
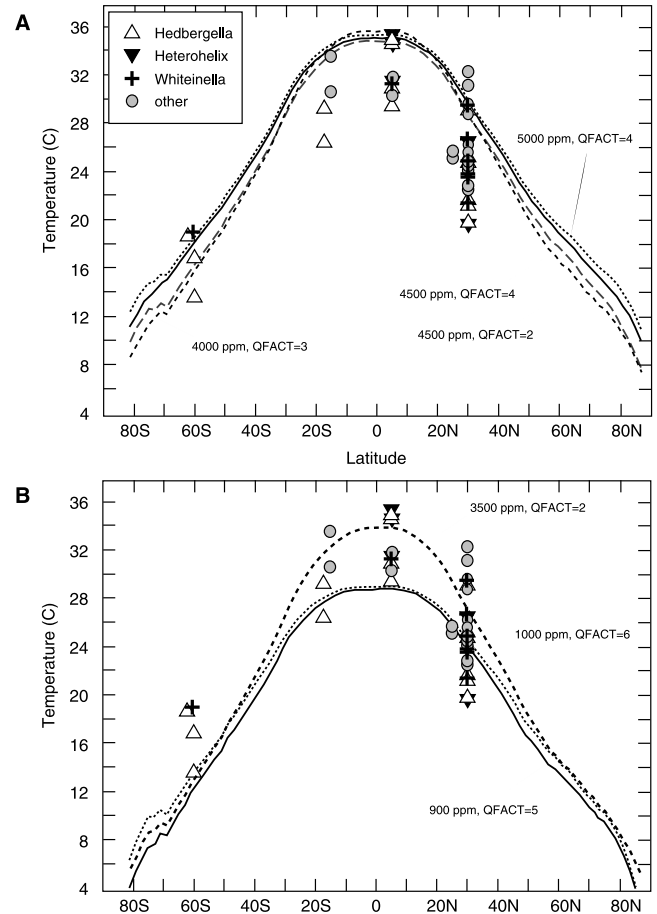

Figure 4. Comparison of GENESIS annual mean zonal ocean surface temperature profiles and upper ocean temperatures calculated from planktonic foraminifera (Figure 3b). (a) Attempts to match maximum temperatures. (b) Attempts to match the minimum temperatures and the maximum gradient allowable by the compiled data. With the exception of Turonian Site 511 values, which have been excluded from this figure, the paleotemperature estimates shown are the same as those shown in Figure 3b. Here, the data are categorized according to general taxonomic groups rather than age.

ments. Ocean model surface forcings were taken from GENESIS runs with 900 ppm CO$_2$ (QFACT = 5) and 4500 ppm CO$_2$ (QFACT = 4) because of their close fit to extremes in reconstructed upper ocean paleotemperatures (Figure 4) (see section 4.1). The ocean model includes a crude bathymetry modified from Albian and Turonian reconstructions used by *Poulsen* [1999].

[20] For each set of boundary conditions, an ocean model run was integrated for at least 18,000 model years using "mixed thermohaline surface boundary conditions" [e.g., *Bryan*, 1986; *Weaver and Sarachik*, 1991; *Marotzke and Willebrand*, 1991]. We assume that surface air temperature, surface winds, and the surface freshwater exchange are controlled by the atmosphere and examine what ocean circulation could exist in equilibrium with the surface forcings. Surface air temperatures and eastward wind

stresses at the surface were averaged zonally for the last 5 years of 30–40 year GENESIS runs. To obtain a moisture flux forcing, evaporation minus precipitation rate (m yr^{-1}) was calculated and then interpolated to 4° horizontal resolution, with a small global correction applied as necessary to maintain a net zero global moisture flux. The resulting moisture flux field was then compared against the land/sea mask prepared for the ocean model. Net precipitation over the continents was summed and redistributed evenly to all ocean areas and the resulting field was averaged zonally. This "global correction" represents an unrealistic treatment of continental runoff, but assures a global moisture flux balance. The implications of this parameterization were considered by *Bice et al.* [1997] and *Bice and Marotzke* [2001]. A simple relaxation condition for SSTs (Newtonian damping toward zonally averaged surface air temperature) is used as an approximation to the more complicated bulk formulae that use SST, surface air temperature, wind speed, and static stability. Similarly, the assumption of annual mean forcings allows us to simplify the question of plausible Cretaceous ocean circulation regimes. While the seasonal cycle is important in water mass formation, omitting it constitutes a quantitative, rather than a qualitative, simplification [*Myers and Weaver*, 1992]. In the ocean, water mass properties are set in late winter, when convection reaches deepest. Omitting the seasonal cycle from the thermal forcing, therefore, is best interpreted as a "perpetual late winter" scenario, rather than forcing with the annual mean. Given the uncertainties in the forcing of any MK ocean model, we consider this idealization minor.

4. Model Results

4.1. Atmospheric Model Results

[21] With solar luminosity reduced by 1% from the modern, model CO$_2$ concentrations of 4500–5000 ppm and a QFACT value of at least 4 are required to obtain ocean surface temperatures comparable to the warmest values inferred from the compiled planktonic data (Figure 4a). Minimum estimated temperatures are approximated by a simulation with 900 ppm CO$_2$ and QFACT = 5 (Figure 4b). An intermediate CO$_2$ concentration of 3500 and QFACT = 2 results in an SST profile intermediate to the match to maximum and minimum temperatures and so produces a profile near the maximum gradient allowable by the compiled upper ocean data (Figure 4b).

[22] Figure 5a shows the relationship between specified atmospheric CO$_2$ concentration and global mean surface temperature for all AGCM simulations performed in this study. Reasonable minimum (900 ppm) and maximum (4500 ppm) CO$_2$ cases have mean global surface temperatures of ∼21°C and 28°C, respectively. Global albedo values for these two experiments are 28.3% and 27.0%, resulting in greenhouse effects of +38.5° and +44.3°C, respectively. These values are ∼6°C and 11°C greater than the modern greenhouse effect of +33°C.

[23] A 1% reduction in solar luminosity results in ∼2.0°C cooling (e.g., data points circled for CO$_2$ = 1000 ppm in Figure 5a). The role of heat distribution in determining global mean surface temperature is apparent: For any given CO$_2$ concentration, increasing the magnitude of the diffusion
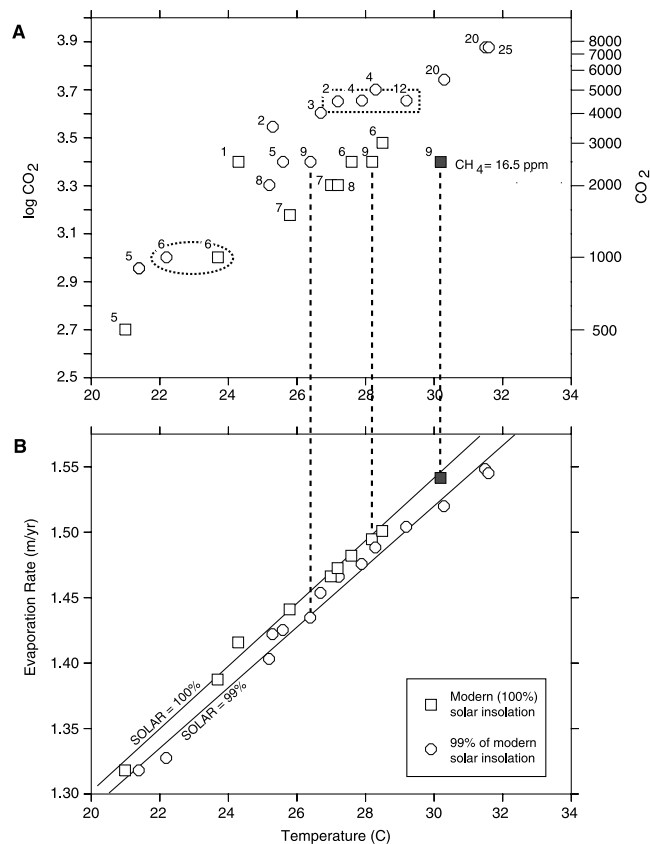

Figure 5. Summary of atmospheric model results. (a) Relationship between model CO$_2$ concentration and annual mean global surface temperature. Symbol labels indicate the model QFACT values specified. (b) Global mean evaporation rate as a function of annual mean global surface temperature. All experiments used 1.65 ppm CH$_4$ with the exception of an elevated CH$_4$ experiment, indicated by the filled symbol. See text for the meaning of other lines shown.

coefficient in the slab ocean heat transport parameterization (QFACT) not only reduces the meridional temperature gradient (see profiles for 4500 ppm CO$_2$ in Figure 4a), but also increases the global mean T (e.g., data points boxed for CO$_2$ = 4500 ppm in Figure 5a). When QFACT is increased at the lower CO$_2$ concentrations, a reverse snow and ice albedo feedback operates to increase the mean surface temperature. This feedback disappears at CO$_2$ and QFACT combinations resulting in polar temperatures consistently above 0°C (under conditions described below). In addition, although the redistribution of heat resulting from increased poleward heat transport leads to tropical cooling (and consequent decreased evaporation and latent heat flux in the tropics), this is more than compensated for by greater warming (and increased evaporation and latent heat flux) poleward of ∼30° latitude. This water vapor greenhouse mechanism operates to increase the global mean temperature with increasing QFACT even after the ice–albedo feedback is gone. Possible Cretaceous climate change implications of this response are discussed in section 5.3.

[24] In Figure 5b, the response of the model hydrologic cycle and atmospheric water vapor is shown by the clear

linear relationship between mean surface temperature and evaporation (or precipitation) rate. The global mean evaporation rate in the 4500 ppm CO_2 (QFACT = 4) case is increased ~12% relative to the 900 ppm CO_2 (QFACT = 5) case. This rate of increase is nearly identical to that obtained using a coupled model and future CO_2 increase scenarios [Dai et al., 2001]. Lines fit to the modern and reduced luminosity data points have similar slopes but different intercepts: for any given mean surface temperature, the reduced solar luminosity case has a lower mean evaporation rate. This occurs because evaporation rate is ultimately limited by the amount of energy received in the form of sunlight. If the ratio between sensible and latent heat loss from the ocean surface (the Bowen Ratio) is the same for both luminosity values, then the lower luminosity case must have a lower evaporation rate. This effect and cooling due to decreased solar flux together produce a 4–5% reduction in the mean evaporation rate with a 1% reduction in solar luminosity.

[25] Figure 5 also illustrates the effect of a 10-fold increase in atmospheric methane concentration in the model. The effect of increasing CH_4 from 1.65 to 16.5 ppm has about the same effect on mean surface temperature and evaporation rate (but opposite sign) as a 1% reduction in solar luminosity (compare data points indicated by vertical dashed lines in Figure 5). Obviously, if atmospheric CH_4 concentrations were higher in the MK, then we would need less CO_2 to produce reasonable matches to minimum and maximum temperature estimates. Unfortunately there is currently no proxy indicator for atmospheric methane and it is unclear how much more CH_4 might be reasonable on either short or long timescales during the MK. The residence time of methane in the atmosphere today is ~8 years and is expected to increase by less than 1 year, given anthropogenic changes projected over the next 50 years [Lelieveld et al., 1998]. If carbon fluxes and reservoir sizes were comparable in the MK, a significantly higher atmospheric methane concentration might be a reasonable boundary condition only for short-lived events such as the <1 Myr interval at the beginning of early Aptian Oceanic Anoxic Event 1a [Jahren et al., 2001; van Breugel et al., 2002] where the size of the carbon isotope excursion and biomarker $\delta^{13}C$ values are consistent with seafloor hydrate destabilization. In the modern Earth, the seafloor methane carbon reservoir is ~3 orders of magnitude larger than the terrestrial methane reservoir. If this relative size difference between reservoirs holds for the MK, then the seafloor hydrate methane reservoir is seemingly capable of producing a significant increase in atmospheric CH_4 only on timescales much shorter than 1 Myr.

[26] The predicted continental climate poleward of 60° latitude varies with values of both CO_2 concentration and QFACT. The following generalizations are made for runs with solar luminosity set at 99% of modern and are based on the temperature criteria in the biome classification scheme of Ziegler [1990]. At QFACT values less than 9 and CO_2 concentrations less than 4000 ppm, predicted polar continental climates are cool or cold temperate: the winter minimum temperature is −1°C to −7°C and average monthly temperatures are above 10°C during fewer than 6 months of the year. Winter precipitation falls as snow, but no snow survives summer melting in either hemisphere. In midwinter, monthly mean snow depths are less than 1.5 m. These cooler polar climates predicted with lower CO_2 and/or low heat transport coefficients are consistent with interpretations of northern polar Albian–Cenomanian paleobotanical evidence by Spicer and Parrish [1986].

[27] At CO_2 concentrations >4000 ppm and QFACT values <10, continental climates poleward of 60° are warm temperate: the winter minimum temperature is above freezing and at least 6 months of the year have mean temperatures above 10°C. In simulations performed with QFACT >10 and CO_2 concentrations of 4500–7500 ppm, the resulting polar continental climates have winter minimum temperatures of 7°C or more and summertime continental maximum temperatures of up to 32°C. The model predictions of warm temperate (and warmer) polar climates are consistent with Cenomanian–Coniacian circum-Arctic botanical and vertebrate fossil evidence [Spicer and Parrish, 1990; Askin and Spicer, 1995; Herman and Spicer, 1996; Tarduno et al., 1998]. Few interpretations of southern polar continental climates exist, but Askin and Spicer [1995] infer fluctuating cool temperate and warm temperate climates for the Cenomanian–Turonian southern high latitudes, a range encompassing most of the simulations performed here.

4.2. Ocean Model Results

[28] The MOM2 ocean model was forced with output from two Cretaceous AGCM simulations whose surface temperature profiles roughly bracket isotopic paleotemperatures from planktonic foraminifera (Figure 4): 900 ppm CO_2 (QFACT = 5) and 4500 ppm CO_2 (QFACT = 4). The high latitude continental climates predicted by the AGCM for these two cases are cool temperate and warm temperate, respectively. The ocean model was forced with annual mean zonal surface conditions, as described in section 3.2. Figure 6 shows the vertical temperature profiles predicted by the ocean model for each site listed in Tables 1 and 2, along with paleotemperatures calculated from planktonic and benthic foraminiferal $\delta^{18}O$, as described in section 2. The model-predicted temperatures bracket both upper ocean and bottom water temperatures inferred from oxygen isotope data, except on Blake Nose at 500 m depth. Here, at Site 1052, the heaviest late Albian shallow benthic foraminiferal values indicate temperatures that are ~7°C cooler than those predicted by the 900 ppm CO_2 case. This difference exceeds the 3°C uncertainty estimate made (see section 2.2) assuming likely deviations in bottom water δ_w from the estimated global mean of −1.0‰ SMOW.

[29] If Blake Nose planktonic foraminifera added secondary calcite below the euphotic zone, as do many modern planktonics (discussed below), then the surface to several hundred meters is a plausible apparent calcification depth range for these specimens. Between 0 and 400 m depth, the 900 ppm CO_2 case encompasses nearly all the Blake Nose planktonic temperature estimates (Figure 6a). The model also matches paleotemperatures for the two deeper sites on Blake Nose well. The reason for the mismatch to the coolest estimates at 500 m is therefore not obvious. If the model is too warm at 500 m on Blake Nose, this might indicate that it
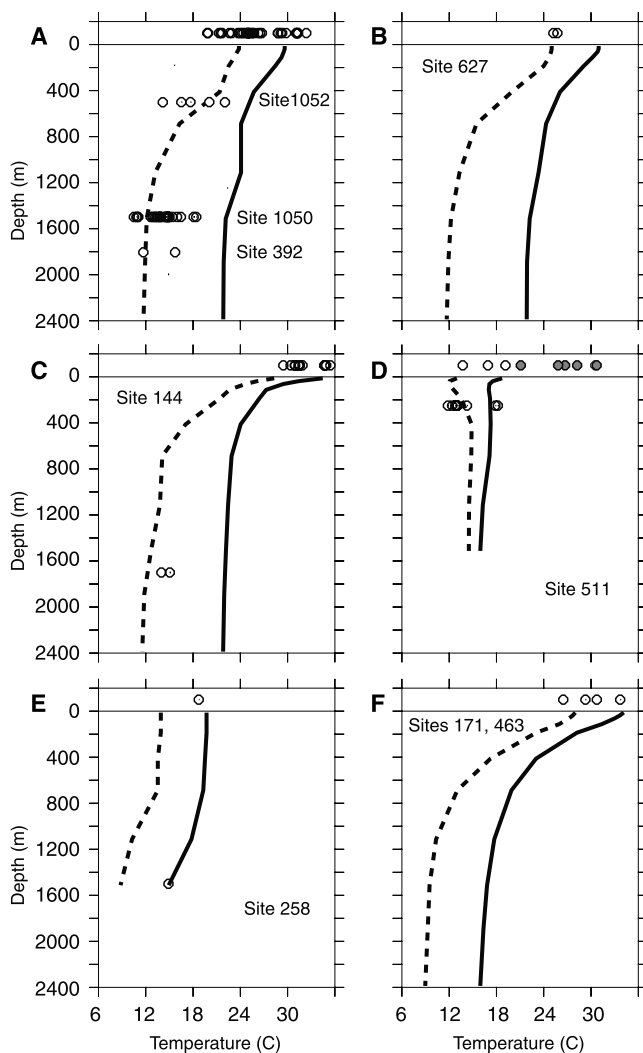
Figure 6. Vertical temperature profiles at each site from which isotopic data were compiled. Profiles are from the 900 ppm CO_2 case (dashed line) and 4500 ppm case (solid line). Bottom water temperatures inferred from benthic $\delta^{18}O$ values are plotted at the paleodepth given in Table 2. Upper ocean temperatures from planktonic data are plotted in the space above 0 m depth. For Site 511, the problematic Turonian planktonic temperatures are indicated by filled symbols. The estimated uncertainties in paleotemperatures from benthic data are $\pm3.0°C$ above 600 m depth and $\pm1.3°C$ at the deeper depths shown (see section 2.2).

underpredicts the strength of local upwelling. Details of the differences between ocean circulation for the 900 and 4500 ppm ocean model cases are discussed below in section 5.2.

5. Discussion
5.1. MK CO_2 Values and Variability

[30] The results of the atmosphere and ocean model indicate that, from the perspective of surface and ocean temperatures, nearly the entire range of MK CO_2 reconstructions (Figure 1) is supported. While there is almost certainly

error associated with each paleo-CO_2 proxy method used [*Retallack*, 2001; *Royer et al.*, 2001], the climate models suggest the possibility that, rather than contradicting one another, the proxy records with moderate and high temporal resolution (10^4 years and less) may sample a record with high variability in atmospheric CO_2, ranging, we estimate, from ~900 to ~5000 ppm. It might be tempting to discount the very high pCO_2 estimates derived from the SI of Siberian *Ginkgo* fossil leaves because they are not corroborated by another proxy technique and because the nonlinear SI/CO_2 relationship is uncalibrated at CO_2 concentrations higher than 560 ppm [*Retallack*, 2001]. However, if the GENESIS climate model is an adequate tool for reconstructing warmer-than-modern climates, then CO_2 concentrations of 4500–5000 ppm are supported because that is what it takes to match the warmest upper ocean paleotemperatures inferred from MK planktonics (excluding for now the Turonian Site 511 data). This fact does not in itself provide support for the SI proxy technique, which should be validated for high CO_2 concentrations independently of any climate model. It is much more difficult to define with confidence the lower bound of CO_2 concentrations using a match to the coolest upper ocean values (for reasons discussed in section 6), but our 900 ppm estimate is consistent with MK CO_2 reconstructions from more than one proxy method (Figure 1). Minimum and maximum CO_2 extremes estimated here could be lowered somewhat if it is proven that atmospheric methane concentrations were significantly higher in the Cretaceous.

[31] From the perspective of the carbon cycle, are the estimated CO_2 extremes plausible? An atmospheric CO_2 concentration of 4500 ppm (~16 times the preindustrial value) would be consistent with a much greater source (primarily volcanic outgassing) and smaller sink (continental weathering) than the modern [*Arthur et al.*, 1985]. Calculations made using an idealized carbon cycle model [after *Berner et al.*, 1983] indicate that 35% greater seafloor spreading rate and a 25% reduction in continental area would allow 4000–4500 ppm CO_2 at steady state. *Larson* [1991] showed that oceanic crust production rates were as much as 75% greater in the MK than they are today, well beyond what is needed to produce 4500 ppm or more atmospheric CO_2 in the idealized carbon model. *Haq et al.* [1987] estimate eustatic sea level to have been higher during the Turonian than at any other time during the past 250 million years. High global sea level is consistent with high mid ocean ridge volume (and high seafloor spreading rates), ocean thermal expansion and low continental surface area (hence low silicate weathering rates). These conditions are in turn consistent with high atmospheric CO_2 and extreme warmth. Our minimum estimate of 900 ppm CO_2 is still consistent with idealized carbon cycle calculations given the lower bounds of estimates of continental area and seafloor spreading rates for the MK [*Berner et al.*, 1983].

[32] We suggest that variations in atmospheric CO_2 of several thousand ppm may have occurred within the 16 Myr window from which temperature data were compiled. Are such variations feasible on the timescale of, say, several million years or less? Given modern reservoir sizes and fluxes, the residence time for CO_2 in the combined atmosphere–ocean system is about 0.5 Myr [*Kasting and Walker*,

1992]. Larger MK ocean and atmosphere carbon reservoir sizes alone would tend to increase the characteristic response time of the atmosphere to changes in fluxes, but, if higher seafloor spreading rates and generally faster recycling rates for inorganic carbon are reasonable for the MK, then the residence time of CO_2 in the MK atmosphere may not have been much longer than today. It is therefore possible to postulate significant CO_2 variability within the 16 Myr interval considered here. Indeed, *Kuypers et al.* [1999] infer a 40–80% decrease in atmospheric CO_2 concentration in as little as 60 kyr across the Cenomanian/Turonian boundary Oceanic Anoxic Event 2.

[33] As was mentioned in section 2, the extremely light $\delta^{18}O$ data from Turonian planktonic foraminifera described by *Huber et al.* [1995] in Site 511 are problematic. If the data do not reflect extreme isotopic depletion of ambient water or diagenetic alteration, the isotopic record indicates upper ocean temperatures of $\sim$26–31°C (given the assumptions in section 2.1). Taken together, the warmest inferred Turonian temperatures in our compilation indicate a pole-to-equator gradient of no more than 10°C. To determine what boundary conditions would be required to fit a SST curve to maximum temperatures estimated from all Turonian data in Table 1 (including Site 511), we ran the atmospheric model with 4500–7500 ppm CO_2 and QFACT values of 12–25. The planktonic foraminifer data are best matched by summer maximum temperatures when 6500–7500 ppm CO_2 and a heat transport coefficient of 15–20 are used. However, when mean annual output from a 7500 ppm AGCM run (with QFACT = 25) is used to force the ocean model, bottom water temperatures at Sites 144 and 511 exceed those estimated from benthic isotope data (Table 2) by 10–14°C. As would be expected, nowhere in the model ocean does the vertical temperature gradient exceed the pole-to-equator gradient in this surface temperature forcing case ($\sim$13°C). If vertical ocean temperature gradients larger than 13°C are supported by data from a Turonian interval anywhere, then the extremely shallow mean annual SST gradient produced by the 7500 ppm CO_2 case is unsupported for that interval. On the other hand, winter high latitude surface temperatures predicted in the 7500 ppm AGCM case exceed the warmest bottom water temperature estimates from benthic foraminifera by only 2–4°C, so it is possible that an ocean model forced by seasonally varying surface conditions would better match Cretaceous conditions. Unfortunately, few data currently exist for defining Turonian deep ocean temperatures and, therefore, vertical temperature gradients. The isotopic record from Site 511 and its possible climate implications are discussed in greater detail by K. L. Bice et al. (Extreme polar warmth during the Cretaceous greenhouse?: The paradox of the Late Turonian Record at DSDP Site S11, submitted to *Paleoceanography*, 2002).

5.2. A Possible Mechanism for MK Oceanographic Change

[34] The global ocean circulation patterns predicted by the ocean model for the 900 and 4500 ppm CO_2 extremes are similar in that bottom waters form at high latitudes in both cases and no subtropical bottom water source is predicted. Because high latitude upper ocean waters are quite warm, it is not necessary to invoke low latitude deep convection in
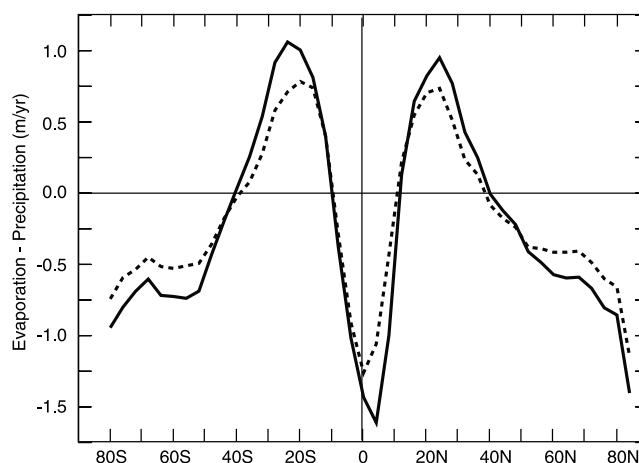

Figure 7. Evaporation minus precipitation (m yr^{-1}) predicted by GENESIS for the 900 ppm CO_2 case (dashed line) and the 4500 ppm case (solid line).

order to reproduce bottom temperatures significantly warmer than modern [*Bice and Marotzke*, 2001]. However, the simulations differ in that the 4500 ppm CO_2 case has a dominant southern Pacific deep water source while the 900 ppm CO_2 case has a strong North Pacific deep water source (Figure 2). In ocean model experiments with modern solar luminosity, 1380 ppm CO_2, and Albian and Turonian paleogeographies, *Poulsen* [1999] obtained only Southern Hemisphere bottom water sources, as did *Brady et al.* [1998] with solar luminosity set at 99.4% of modern, 1680 ppm CO_2 and a Campanian (80 Ma) paleogeography. *Barron and Peterson* [1990], on the other hand, obtained North Pacific deep convection with modern solar luminosity, 340 ppm CO_2 and an Albian-like ocean geometry. *Brady et al.* [1998] and *Poulsen* [1999] speculated that the Northern Hemisphere bottom water source obtained by *Barron and Peterson* [1990] might result from differences in maximum water depth in high northern versus high southern latitudes. However, we obtain two different thermohaline "modes" with the same basin configuration. This suggests that changes in buoyancy forcing could have played a significant role in changing MK ocean circulation.

[35] While the surface temperature values differ significantly between our 900 and 4500 ppm CO_2 cases (Figures 4a and 4b), the meridional temperature gradients and wind stress forcings are similar. The greatest difference in buoyancy forcing between the two cases is in the moisture flux. The zonal mean evaporation minus precipitation rate (E-P) is $\sim$35% greater in the 4500 ppm CO_2 case than in the 900 ppm case (Figure 7). As described by *Bice and Marotzke* [2001, 2002], the primary effect of such an increase is deepened subtropical subduction and the increased transport of warm, saline subtropical water to the high latitudes via boundary currents and shallow overturning. At high latitudes, this saline water may strengthen existing deep convection or force a switch to deep water formation in a site of previous intermediate water formation, depending on the details of the circulation path. *Bice and Marotzke* [2002] obtained such a switch from Southern Hemisphere to Northern Hemisphere

deep water formation at a 60% increase in the E-P profile of a late Paleocene AGCM simulation. A combination of increases in global temperature and E-P related to increases in CO$_2$ contribute to changes in the site of deep water formation in the MK ocean model. These results suggest that carbon cycle-induced changes in CO$_2$, consequent warming/cooling and hydrologic cycle increases/decreases could have driven changes in the strength of deep water production in both hemispheres during the MK, if these extremes in CO$_2$ are realistic. This result is consistent with the recent results of *Otto-Bliesner et al.* [2002] who, in a Campanian coupled model, obtained both Southern and Northern Hemisphere sinking, with intensities varying with specified CO$_2$ concentration. Variations in deep water flows have implications for both the distribution of deep ocean temperatures and oxygen concentrations, and the distribution and stability of gas hydrates, among other variables [*Bice and Marotzke*, 2002].

5.3. Hydrologic Cycle Responses to Temperature Gradient Change

[36] As was noted in section 4.1, an increase in the magnitude of the diffusion coefficient in the slab ocean heat transport parameterization (QFACT) reduces the surface temperature gradient and increases global mean surface temperature. *Rind* [2000] outlined suggestive rules for climate change expected to accompany changes in SST gradient. Using an atmospheric GCM similar to GENESIS with specified SSTs, Rind examined the effect of decreasing the SST gradient while increasing the global mean surface temperature (by increasing SSTs at all latitudes). The tropical warming led to a wetter atmosphere, from which Rind concluded that "To dry the global atmosphere, tropical temperatures must be colder" and the inverse; To make a wetter atmosphere, tropical temperatures must be warmer.

[37] It is important to note, however, that all our sensitivity experiments in which only QFACT was increased represent a case not examined by *Rind* [2000] and one that contradicts this generalization regarding reduced gradients in a globally warmer climate. When we increase the poleward heat transport coefficient and hold all other boundary conditions constant, tropical temperatures decrease, but extratropical temperatures increase by a relatively greater amount. Hence, the mean global evaporation rate increases and global mean temperature increases. This case results in a wetter atmosphere despite the fact that tropical temperatures decrease. The sense of change (warming at all latitudes) imposed by *Rind* [2000] matches the change inferred between the modern and MK climates (Figure 3b) but may not resemble climate change *within* a warm climate interval. Our experiments indicate that a wetter atmosphere may accompany relative tropical cooling if coincident, greater extratropical warming also occurs. This is important to keep in mind when trying to understand the global implications of emerging records of high frequency climate variability within the Cretaceous itself [e.g., *Wilson and Norris*, 2001] where smaller-scale SST gradient changes may have occurred.

6. Limitations and Uncertainties

[38] Given general model limitations, broad uncertainties in the boundary conditions specified to the models and so

few data against which to compare model results, it is important to consider the uncertainties in these results. For the atmospheric model, the critical limitation here may be that associated with increased greenhouse gases themselves. Most importantly, the model sensitivity to increased CO$_2$ is largely determined by water vapor and cloud feedbacks, which are in turn dependent on the specified cloud parameterization [*Cess et al.*, 1990]. The same experiments performed using different GCMs will result in higher or lower estimated CO$_2$ extremes than those derived using GENESIS. In addition, as with many GCMs, the GENESIS model may be deficient in capturing the full suite of chemical feedbacks stemming from higher atmospheric CO$_2$ and CH$_4$ [*Lelieveld and Crutzen*, 1992]. Although the direct radiative effects of CO$_2$ and methane are included in the GENESIS code, the true temperature and chemical effects of increased CO$_2$ and CH$_4$ are likely to be underestimated. For example, the model lacks the feedback of CO$_2$ on stratospheric water vapor content and circulation that would otherwise give rise to optically thicker polar stratospheric clouds and increased high latitude surface heating [*Sloan and Pollard*, 1998; *Kirk-Davidoff et al.*, 1999, 2002]. A better representation of these processes in the model should cause a decrease in the poleward heat transport coefficient (QFACT) required to produce a reasonable match to inferred high latitude temperatures. It is therefore possible that QFACT, at least in part, represents a tuning that compensates for a model atmospheric deficiency. This possibility is supported by the fact that the ocean heat transport predicted by the ocean model is less than that implied by the atmospheric model (see section 3.1). Several studies [*Poulsen*, 1999; *Bice et al.*, 2000] have illustrated this discrepancy that indicates that the role of the atmosphere in sustaining warm high latitudes and continental interiors has been underestimated [*Sloan et al.*, 1995]. *Emanuel* [2001, 2002] has proposed a plausible mechanism for increased poleward heat transport during a greenhouse climate that involves increases in both atmosphere and ocean transport in response to increased storm frequency and intensity [e.g., *PSUCLIM*, 1999a, 1999b] and a deepened mixed layer [e.g., *Bice and Marotzke*, 2001] in a greenhouse world.

[39] Another point to bear in mind is that surface temperatures predicted by an atmospheric model with a nondynamical "slab" ocean, such as GENESIS, can not be compared directly to isotopic paleotemperatures from planktonic foraminifera. The AGCM slab ocean does not include the temperature effects of ocean circulation and therefore can not predict the temperatures of waters recorded by planktonic foraminifera. This point is especially important in the comparison of tropical and subtropical temperatures where upper ocean waters are dramatically cooled by Ekman divergence and upwelling associated with the persistent trade winds [*Levitus*, 1982]. The temperature effects of this upwelling are captured by dynamical ocean circulation models such as MOM2. When forced by output from Cretaceous and Paleogene AGCM simulations with warm tropics, tropical ocean temperatures in the uppermost 500 m of the dynamical ocean model in fact compare well with "cool" isotopic
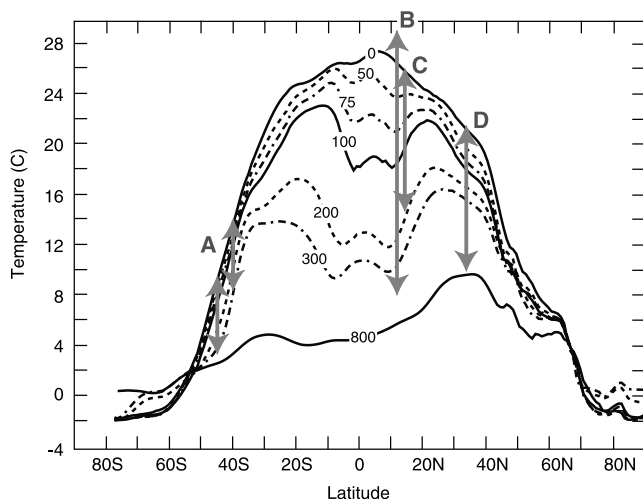
Figure 8. Contours of modern Atlantic mean temperatures between 60°W and 10°W longitude at 0–800 m depth [*Levitus*, 1982]. Profile labels are water depth (m). Vertical arrows indicate the range of temperatures recorded by modern planktonic foraminifera: (a) *Neogloboquadrina pachyderma, Globigerinoides sacculifer,* and *Globorotalia truncatulinoides* in the South Atlantic [*Niebler et al.*, 1999], (b) *Globigerinoides sacculifer* and *G. ruber* in the tropical Indian Ocean [*Duplessy et al.*, 1981], (c) *Globortalia menardii* in the tropical North Atlantic (R. Norris, unpublished data), and (d) *Hastigerina, Globigerina, Globigerinoides,* and *Globorotalia* (12 total species) in the Sargasso Sea [*Erez*, 1979].

paleotemperatures (Figure 6) [*Poulsen et al.*, 1999b; *Bice et al.*, 2000].

[40] Problems associated with the reconstruction of Cretaceous water temperature from biogenic carbonate include the assumption of equilibrium fractionation in extinct species, possible diagenesis, and uncertainty in the true δ_w value. We assume that planktonic foraminifera calcify approximately in isotopic equilibrium with seawater, an assumption borne out in general terms by most studies of modern planktic foraminifera. However, the assumption of isotopic equilibrium is confounded by the tendency of many modern foraminifera to grow their primary chamber calcite in surface waters but then add varying amounts of gametogenic or "secondary" calcite late in the life cycle at thermocline or subthermocline depths. The result of ontogenetic changes in depth habitat therefore result in an average shell chemistry that does not reflect actual surface temperatures (Figure 8). It is not known the extent to which Cretaceous foraminifera underwent ontogenetic changes in depth like their modern counterparts. Calcite morphologies resembling the gametogenic material added, for example, by modern *Globorotalia* are not recognized in Cretaceous samples, but we can not exclude the possibility that some Cretaceous taxa may have added a thin gametogenic crust like modern *Globigerinoides ruber*. Some thermocline species, such as Albian/Cenomanian *Rotalipora* apparently did not change depth habitats [e.g., *Norris and Wilson,*

1998], but there has been little work on this subject in other Middle and Late Cretaceous planktonic foraminifera. Addition of gametogenic calcite in Upper Cretaceous species could partly account for the "Cool Tropics Paradox" [*D'Hondt and Arthur*, 1996] by causing isotopic measurements of planktonic foraminifera to underestimate actual upper ocean water temperatures.

[41] Uncertainties in the actual depth habitat of various species could also contribute to underestimates of true SSTs. For example, some species such as *Hedbergella delrioensis* and *Heterohelix moremani* appear to have an opportunistic habitat, sometimes growing in the surface ocean and other times recording subsurface conditions [e.g., *Premoli-Silva and Sliter*, 1999; *Norris and Wilson*, 1998; *Wilson et al.*, 2002]. In the tropical ocean, this effect, combined with the pronounced cooling due to upwelling (Figure 8) may have also contributed to the apparent "Cool Tropic Paradox."

[42] Nonequilibrium calcification could also reflect variations in surface ocean pH and carbonate ion concentration. Culture experiments with living planktonic foraminifera demonstrate that $\delta^{18}O$ in foraminifer calcite increases with decreasing pH and carbonate ion concentration [*Spero et al.*, 1997]. The higher pCO_2 suggested for the MK atmosphere and surface ocean would reduce surface pH and cause foraminiferal $\delta^{18}O$ to underpredict true upper ocean temperatures [*Zeebe*, 2001]. If the high CO₂ concentrations suggested by our simulations are realistic, upper ocean temperatures determined from foraminifer $\delta^{18}O$ underestimate the true temperatures, thereby requiring even higher CO₂ to explain actual tropical paleotemperatures.

[43] We have tried to eliminate data from possible altered carbonate material based on published opinions and visual inspection, preferring to use foraminifera with a glassy, translucent appearance, preserved ornamentation and interior chamber walls, and open pores. But the possibility remains of subtle alteration of original $\delta^{18}O$ due to diffusion of oxygen isotopes under high burial temperatures and the addition of minor diagenetic calcite. For low latitude planktonic foraminifera, addition of diagenetic calcite in equilibrium with either bottom water or shallow pore waters results in an increase in carbonate $\delta^{18}O$ and artificially low temperature estimates [*Milliman*, 1966; *Schrag et al.*, 1995; *Pearson et al.*, 2001]. Actual tropical and subtropical upper ocean temperatures would be higher than those shown in Figure 3b if diagenetic calcite has been added on the seafloor or at very shallow burial depths. Higher CO₂ and/or lower QFACT values would then be required for the model to match actual paleotemperatures.

[44] Uncertainties exist in both the actual global mean water $\delta^{18}O$ value and in any latitude-dependent adjustment for upper ocean waters. We have assumed the "ice-free" ocean value of −1‰ (SMOW) used in most previous Cretaceous paleotemperature estimates [*Shackleton and Kennett*, 1975]. However, this calculation was based only on ice mass balance estimates and does not include the long-term increase in hydrosphere $\delta^{18}O$ [*Wallmann*, 2001b] due to the surplus source of ^{18}O (primarily high temperature seafloor alteration) over sinks (continental weathering, low

temperature seafloor alteration, water fixation in the upper oceanic crust and in clay minerals). *Wallmann* [2001b] estimates that the MK ocean would have been depleted ~0.25‰ beyond the ice-free value, yielding a MK ocean mean of −1.25‰. Using this value would decrease all our temperature calculations by ~1.2°C and gradients would remain unchanged. Lower CO$_2$ would then be required for the model to match actual paleotemperatures.

[45] The assumption of a modern-like latitude−δ$_w$ gradient [*Zachos et al.*, 1994] may be inappropriate for the warmer MK intervals because of the stronger hydrologic cycle and lower meridional temperature gradients. In low latitudes, higher evaporation rates would result in less fractionation of oxygen isotopes, so that tropical surface waters would be left less enriched with respect to ^{18}O and would look more like the mean ocean value than do modern tropical surface waters. Decreased fractionation between condensate and water vapor with increased Intertropical Convergence Zone precipitation rates would further buffer tropical surface water toward the global mean. Rayleigh distillation of the lighter isotope would still be expected along the predominant water vapor path from low to high latitudes, but, because the initial source water vapor looks more like the mean ocean value, high latitude precipitation and surface water δ^{18}O would likely also look more like the mean value. Therefore, precipitation, runoff, and high latitude surface ocean water might be less depleted in the MK than it is today. The net effect of increased hydrologic cycle rates might therefore be to reduce the pole-to-equator surface ocean δ$_w$ gradient relative to the modern. *Jouzel et al.* [2000] predict a lower meridional gradient in precipitation δ^{18}O for a 2 × CO$_2$ climate using an AGCM that includes water isotopes. The Jouzel et al. model predicts less depleted high latitude precipitation in the warmer climate, a result recently supported by precipitation δ^{18}O inferred from Eocene Arctic fossil wood [*Jahren and Sternberg*, 2002].

[46] If the effect of increased high latitude freshwater δ^{18}O is not compensated for by a substantially increased high latitude freshwater flux, then a decreased gradient in precipitation δ^{18}O will lead to a decreased gradient in δ$_w$. In the isotopic paleotemperature calculations, the result of a smaller upper ocean δ$_w$ gradient would be to decrease low latitude and increase high latitude upper ocean temperature estimates. Somewhat higher model QFACT values than ours would be required in order to match upper ocean paleotemperatures adjusted for a lower δ$_w$ gradient in the warm MK climate.

[47] *Poulsen et al.* [1999b] and *Bice et al.* [2000] both examine the potential use of ocean model predicted salinities to calculate Cretaceous and Paleogene δ$_w$ values. The severe limitation to this approach is in the choice of a salinity−δ$_w$ relationship from several modern observed relationships. Calculating δ$_w$ from the model-predicted mixed-layer salinities at the tropical sites used here has the effect of leaving the isotopic paleotemperature unchanged (relative to the temperatures shown in Figure 3b), cooling it by 1−4°C, or warming it by 1°C, depending on which salinity−δ$_w$ relationship is used [*Broecker*, 1989; *Fairbanks et al.*, 1992; *Woo et al.*, 1992]. Attempting to

relate δ$_w$ values (or δ$_w$ change) directly to salinity (or salinity change) is therefore not wise.

[48] Finally, we note that a MK CO$_2$ level lower than 900 ppm would better match the minimum inferred temperatures on Blake Nose (Figure 4b). It is worth considering an even cooler MK world because of local records interpreted as consistent with ice sheet growth and decay in the Cenomanian [*Stoll and Schrag*, 2000]. Decreasing the model CO$_2$ concentration below 900 ppm and/or lowering QFACT value below 5 would result in a better match to the coolest data on Blake Nose, but the resulting cooler surface temperature profile would be unconstrained elsewhere, given current data (Figure 4b). At some point with decreasing CO$_2$ in the model, the predicted summer temperatures on the high latitude continents will result in snow survival through summer [*Gibbs et al.*, 2000] and, if snowfall exceeds summer melt, the growth of high latitude ice sheets would be supported by the atmospheric model.

7. Concluding Statement

[49] The existence of foraminifer isotopic data suggestive of tropical and temperate SSTs in excess of 30°C demands CO$_2$ concentrations of 4500 ppm or more. In contrast, minimum temperatures recorded by MK planktonic foraminifera do not provide tight constraints on CO$_2$ since low temperature estimates can result from a number of factors, ranging from tropical upwelling and possible secondary calcification to variations in the depth ecology of the foraminifera. However, if claims for MK glacial eustacy can be upheld, we would have strong evidence that the CO$_2$ in the atmosphere must have been highly dynamic, as is already suggested by the results presented here and by the wide range of atmospheric CO$_2$ proxy data. To demonstrate that the range in existing CO$_2$ estimates from proxy data and carbon cycle models reflects high amplitude variability in the record would require either multiproxy studies focused on coeval terrestrial and marine sediment sections, if such correlations can be made within relatively restricted MK time intervals, or high temporal resolution sampling of well-dated marine sequences. Since ocean GCMs only support high latitude deep water formation in this warm climate interval, more and better distributed benthic foraminiferal δ^{18}O data will help to better constrain plausible high latitude upper ocean temperatures.

References

Arthur, M. A., W. E. Dean, and S. O. Schlanger, Variations in the global carbon cycle during the Cretaceous related to climate, volcanism, and changes in atmospheric CO$_2$, in *The Carbon Cycle and Atmospheric CO$_2$: Natural Variations Archean to Present*, Geophys. Monogr. Ser., vol. 32, edited by E. T. Sundquist and W. S. Broecker, pp. 504–530, AGU, Washington, D. C., 1985.

Askin, R. A., and R. A. Spicer, The late Cretaceous and Cenozoic history of vegetation and climate at northern and southern high latitudes: A comparison, in *Effects of Past Global Change on Life*, edited by S. M. Stanley, pp. 22–25, Natl. Acad. Press, Washington, 1995.

Barron, E. J., Cretaceous plate tectonic reconstructions, *Palaeogeogr. Palaeoclimatol. Palaeoecol.*, *59*, 3–29, 1987.

Barron, E. J., and W. H. Peterson, Mid-Cretaceous ocean circulation: Results from model sensitivity studies, *Paleoceanography*, *5*, 319–337, 1990.

Barron, E. J., W. H. Peterson, D. Pollard, and S. L. Thompson, Past climate and the role of ocean heat transport: Model simulations for the Cretaceous, *Paleoceanography*, *8*, 785–798, 1993a.

Barron, E. J., P. J. Fawcett, D. Pollard, and S. L. Thompson, Model simulations of Cretaceous climates: The role of geography and carbon dioxide, *Philos. Trans. R. Soc. London, Ser. B*, *B341*, 307–316, 1993b.

Barron, E. J., P. J. Fawcett, W. H. Peterson, D. Pollard, and S. L. Thompson, A "simulation" of mid-Cretaceous climate, *Paleoceanography*, *10*, 953–962, 1995.

Beerling, D. J., F. I. Woodward, and P. J. Valdes, Global terrestrial productivity in the mid-Cretaceous (100 Ma): Model simulations and data, in *Evolution of the Cretaceous Ocean–Climate System*, edited by E. Barrera and C. Johnson, Spec. Pap. Geol. Soc. Am., *332*, 385–390, 1999.

Berner, R. A., and E. J. Barron, Comments on the BLAG model: Factors affecting atmospheric CO$_2$ and temperature over the past 100 million years, *Am. J. Sci.*, *284*, 1183–1192, 1984.

Berner, R. A., and Z. Kothavala, GEOCARB III: A revised model of atmospheric CO$_2$ over Phanerozoic time, *Am. J. Sci.*, *301*, 182–204, 2001.

Berner, R. A., A. C. Lasaga, and R. M. Garrels, The carbonate–silicate geochemical cycle and its effects on atmospheric carbon dioxide over the past 100 million years, *Am. J. Sci.*, *283*, 641–683, 1983.

Bice, K. L., and J. Marotzke, Numerical evidence against reversed thermohaline circulation in the warm Paleocene/Eocene ocean, *J. Geophys. Res.*, *106*, 11,529–11,542, 2001.

Bice, K. L., and J. Marotzke, Could changing ocean circulation have destabilized methane hydrate at the Paleocene/Eocene boundary?, *Paleoceanography*, *17*, 1018, doi:10.1029/2001PA000678, 2002.

Bice, K. L., E. J. Barron, and W. H. Peterson, Continental runoff and early Cenozoic bottom-water sources, *Geology*, *25*, 951–954, 1997.

Bice, K. L., L. C. Sloan, and E. J. Barron, Comparison of early Eocene isotopic paleotemperatures and the three-dimensional OGCM temperature field: The potential for use of model-derived surface water δ^{18}O, in *Warm Climates in Earth History*, edited by B. T. Huber et al., pp. 79–131, Cambridge Univ. Press, New York, 2000.

Brady, E. C., R. M. DeConto, and S. L. Thompson, Deep water formation and poleward ocean heat transport in the warm climate extreme of the Cretaceous (80 Ma), *Geophys. Res. Lett.*, *25*, 4205–4208, 1998.

Broecker, W. S., The salinity contrast between the Atlantic and Pacific Oceans during glacial time, *Paleoceanography*, *4*, 207–212, 1989.

Bryan, F., High-latitude salinity effects and inter-hemispheric thermohaline circulations, *Nature*, *323*, 301–304, 1986.

Cerling, T. E., Carbon dioxide in the atmosphere: Evidence from Cenozoic and Mesozoic paleosols, *Am. J. Sci.*, *291*, 377–400, 1991.

Cess, R. D., et al., Intercomparison and interpretation of climate feedback processes in 19 atmospheric general circulation models, *J. Geophys. Res.*, *95*, 16,601–16,615, 1990.

Cowling, S. A., Plants and temperature: CO$_2$ uncoupling, *Science*, *285*, 1500–1501, 1999.

Crowley, T. J., Remembrance of things past: Greenhouse lessons from the geological record, *Consequences*, 2, U.S. GCRIO [Online], 1996. (Available as http://www.gcrio.org/CONSEQUENCES/winter96/geoclimate.html).

Crowley, T. J., and R. A. Berner, CO$_2$ and climate change, *Science*, *292*, 870–872, 2001.

Dai, A., G. A. Meehl, W. M. Washington, T. M. L. Wigley, and J. M. Arblaster, Ensemble simulation of twenty-first century climate changes: Business as usual versus CO$_2$ stabilization, *Bull. Am. Meteorol. Soc.*, *82*, 2377–2388, 2001.

DeConto, R. M., W. W. Hay, S. L. Thompson, and J. Bergengren, Late Cretaceous climate and vegetation interactions: Cold continental interior paradox, in *Evolution of the Cretaceous Ocean–Climate System*, edited by E. Barrera and C. Johnson, Spec. Pap. Geol. Soc. Am., *332*, 391–406, 1999.

DeConto, R. M., E. C. Brady, J. Bergengren, and W. H. Hay, Late Cretaceous climate, vegetation, and ocean interactions, in *Warm Climates in Earth History*, edited by B. T. Huber et al., pp. 275–296, Cambridge Univ. Press, New York, 2000.

D'Hondt, S., and M. A. Arthur, Late Cretaceous oceans and the cool tropic paradox, *Science*, *271*, 1838–1841, 1996.

Douglas, R. G., and S. M. Savin, Oxygen and carbon isotope analyses of Cretaceous and Tertiary foraminifera from the central north Pacific, *Deep Sea Drill. Proj. Init. Rep.*, *17*, 591–605, 1973.

Duplessy, J.-C., P.-L. Blanc, and A. W. H. Be, Oxygen-18 enrichment of planktonic foraminifera due to gametogenic calcification below the euphotic zone, *Science*, *213*, 1247–1250, 1981.

Ekart, D. D., T. E. Cerling, I. P. Montanez, and N. J. Tabor, A 400 million year carbon isotope record of pedogenic carbonate: Implications for paleoatmospheric carbon dioxide, *Am. J. Sci.*, *299*, 805–827, 1999.

Emanuel, K., Contribution of tropical cyclones to meridional heat transport by the oceans, *J. Geophys. Res.*, *106*, 14,771–14,781, 2001.

Emanuel, K., A simple model of multiple climate regimes, *J. Geophys. Res.*, *107*, 4077, doi: 10.1029/2001JD001002, 2002.

Erez, J., The influence of differential production and dissolution of the stable isotope composition of planktonic foraminifera, Ph.D. thesis, 119 pp., Woods Hole Oceanogr. Inst./Mass. Inst. of Technol. Joint Prog. in Oceanogr. and Ocean Eng., Woods Hole, Mass., 1979.

Erez, J., and B. Luz, Experimental paleotemperature equation for planktonic foraminifera, *Geochim. Cosmochim. Acta*, *47*, 1025–1031, 1983.

Fairbanks, R. G., C. D. Charles, and J. D. Wright, Origin of global meltwater pulses, in *Radiocarbon After Four Decades: An Interdisciplinary Perspective*, edited by R. E. Taylor et al., pp. 473–500, Springer-Verlag, New York, 1992.

Fassell, M. L., and T. J. Bralower, Warm, equable mid-Cretaceous: Stable isotope evidence, in *Evolution of the Cretaceous Ocean–Climate System*, edited by E. Barrera and C. Johnson, Spec. Pap. Geol. Soc. Am., *332*, 121–142, 1999.

Flower, B. P., Warming without higher CO$_2$?, *Nature*, *399*, 313–314, 1999.

Freeman, K. H., and J. M. Hayes, Fractionation of carbon isotopes by phytoplankton and estimates of ancient CO$_2$ levels, *Glob. Biogeochem. Cycles*, *6*, 185–198, 1992.

Ganachaud, A., and C. Wunsch, Improved estimates of global ocean circulation, heat transport and mixing from hydrographic data, *Nature*, *408*, 453–457, 2000.

Garnier, E., B. Barneier, L. Siefridt, and K. Beranger, Investigating the 15-year air–sea flux climatology from the ECMWF re-analysis project as a surface boundary condition for ocean models, *Int. J. Climatol.*, *20*, 1653–1673, 2000.

GEOSECS, *Atlantic, Pacific and Indian Ocean Expeditions, Volume 7, Shorebased Data and Graphics*, IDOE NSF, Washington, D. C., 1987.

Gibbs, M. T., K. L. Bice, G. Jenkins, E. J. Barron, and L. R. Kump, Glaciation in the early Paleozoic "greenhouse": The role of paleogeography and atmospheric CO$_2$, in *Warm Climates in Earth History*, edited by B. T. Huber et al., pp. 386–422, Cambridge Univ. Press, New York, 2000.

Gough, D. O., Solar interior structure and luminosity variations, *Sol. Phys.*, *74*, 21–34, 1981.

Grossman, E. L., and T.-L. Ku, Oxygen and carbon isotope fractionation in biogenic aragonite: Temperatures effects, *Chem. Geol.*, *59*, 59–74, 1986.

Haq, B. U., J. Hardenbol, and P. R. Vail, Chronology of fluctuating sea levels since the Triassic, *Science*, *235*, 1156–1167, 1987.

Herman, A. B., and R. A. Spicer, Palaeobotanical evidence for a warm Cretaceous Arctic Ocean, *Nature*, *380*, 330–333, 1996.

Huber, B. T., D. A. Hodell, and C. P. Hamilton, Middle-Late Cretaceous climate of the southern high latitudes: Stable isotopic evidence for minimal equator-to-pole thermal gradients, *GSA Bull.*, *107*, 1164–1191, 1995.

Huber, B. T., R. M. Leckie, R. D. Norris, T. J. Bralower, and E. CoBabe, Foraminiferal assemblage and stable isotopic change across the Cenomanian-Turonian boundary in the subtropical North Atlantic, *J. Foraminiferal Res.*, *29*, 392–417, 1999.

Huber, B. T., R. D. Norris, and K. G. MacLeod, Deep-sea paleotemperature record of extreme warmth during the Cretaceous, *Geology*, *30*, 123–126, 2002.

Hut, G., Consultants group meeting on stable isotope reference samples for geochemical and hydrological investigations, Rep. to Dir. Gen., Int. At. Energy Agency, Vienna, 42 pp., 1987.

Jahren, H. A., and L. S. L. Sternberg, Eocene meridional weather patterns reflected in the

oxygen isotopes of Arctic fossil wood, *GSA Today*, 12, 4–9, 2002.

Jahren, H. A., N. C. Arens, G. Sarmiento, J. Guerrero, and R. Amundson, Terrestrial record of methane hydrate dissociation in the Early Cretaceous, *Geology*, 29, 159–162, 2001.

Jouzel, J., G. Hoffmann, R. D. Koster, and V. Masson, Water isotopes in precipitation: Data/model comparison for present-day and past climates, *Quat. Sci. Rev.*, 19, 363–379, 2000.

Kasting, J. F. and J. C. G. Walker, The geochemical carbon cycle and the uptake of fossil fuel CO_2, in *Global Warming: Physics and Facts*, edited by B. G. Levi et al., pp. 175–200, Am. Inst. of Phys., New York, 1992.

Kiehl, J. T., and R. E. Dickinson, A study of the radiative effects of enhanced atmospheric CO_2 and CH_4 on early Earth surface temperatures, *J. Geophys. Res.*, 92, 2991–2998, 1987.

Kirk-Davidoff, D. B., E. J. Hintsa, J. G. Anderson, and D. W. Keith, The effect of climate change on ozone depletion through changes in stratospheric water vapour, *Nature*, 402, 399–401, 1999.

Kirk-Davidoff, D. B., D. P. Schrag, and J. G. Anderson, On the feedback of stratospheric clouds on polar climate, *Geophys. Res. Lett.*, 29, 1556, doi:10.1029/2002GL014659, 2002.

Kuypers, M. M. M., R. D. Pancost, and J. S. Sinninghe Damsté, A large and abrupt fall in atmospheric CO_2 concentration during Cretaceous times, *Nature*, 399, 342–345, 1999.

Larson, R. L., Latest pulse of Earth: Evidence for a mid-Cretaceous superplume, *Geology*, 19, 547–550, 1991.

Lelieveld, J., and P. J. Crutzen, Indirect chemical effects of methane on climate warming, *Nature*, 355, 339–342, 1992.

Lelieveld, J., P. J. Crutzen, and F. J. Dentener, Changing concentration, lifetime and climate forcing of atmospheric methane, *Tellus*, 50, 128–150, 1998.

Levitus, S., Climatological atlas of the world ocean: NOAA Professional Paper 13, 173 pp., U.S. Govt. Print. Off., Washington, D. C., 1982.

Manabe, S., Early development in the study of greenhouse warming: The emergence of climate models, *Ambio*, 26, 47–51, 1996.

Marotzke, J., and J. Willebrand, Multiple equilibria of the global thermohaline circulation, *J. Phys. Oceanogr.*, 21, 1372–1385, 1991.

Milliman, J. D., Submarine lithification of carbonate sediments, *Science*, 153, 994–997, 1966.

Myers, P. G., and A. J. Weaver, Low-frequency internal oceanic variability under seasonal forcing, *J. Geophys. Res.*, 97, 9541–9563, 1992.

Niebler, H.-S., H.-W. Hubberten, and R. Gersonde, Oxygen isotope values of planktic foraminifera: A tool for the reconstruction of surface water stratification, in *Use of Proxies in Paleoceanography: Examples from the South Atlantic*, edited by G. Fischer and G. Wefer, pp. 165–189, Springer-Verlag, New York, 1999.

Norris, R. D., and P. A. Wilson, Low-latitude sea-surface temperatures for the mid-Cretaceous and the evolution of planktic foraminifera, *Geology*, 26, 823–826, 1998.

Norris, R. D., et al., Proc. Ocean Drill. Program Init. Rep., Leg 171B, College Station, Tex., 1998.

Norris, R. D., K. L. Bice, E. A. Magno, and P. A. Wilson, Jiggling the tropical thermostat during the Cretaceous hot house, *Geology*, 30, 299–302, 2002.

Otto-Bliesner, B. L., E. C. Brady, and C. Shields, Late Cretaceous ocean: Coupled simulations with the National Center for Atmospheric Research Climate System Model, *J. Geophys. Res.*, 107, 4019, doi:10.1029/2001JD000821, 2002.

Pearson, P. N., P. W. Ditchfield, J. Singano, K. G. Harcourt-Brown, C. J. Nicholas, R. K. Olsson, N. J. Shackleton, and M. A. Hall, Warm tropical sea surface temperatures in the Late Cretaceous and Eocene epochs, *Nature*, 413, 481–487, 2001.

Poulsen, C. J., The mid-Cretaceous ocean circulation and its impact on greenhouse climate dynamics, Ph.D. thesis, 219 pp., Pennsylvania State Univ., University Park, 1999.

Poulsen, C. J., E. J. Barron, C. C. Johnson, and P. J. Fawcett, Links between major climatic factors and regional oceanic circulation in the Mid-Cretaceous, in *Evolution of the Cretaceous Ocean–Climate System*, edited by E. Barrera and C. Johnson, *Spec. Pap. Geol. Soc. Am.*, 332, 73–89, 1999a.

Poulsen, C. J., E. J. Barron, W. H. Peterson, and P. A. Wilson, A reinterpretation of mid- Cretaceous shallow marine temperatures through model-data comparison, *Paleoceanography*, 14, 679–697, 1999b.

Premoli-Silva, I., and W. V. Sliter, Cretaceous paleoceanography: Evidence from planktonic foraminiferal evolution, in *Evolution of the Cretaceous Ocean–Climate System*, edited by E. Barrera and C. Johnson, *Spec. Pap. Geol. Soc. Am.*, 332, 301–328, 1999.

Price, G. D., P. J. Valdes, and B. W. Sellwood, A comparison of GCM simulated Cretaceous "greenhouse" and "icehouse" climates: Implications for the sedimentary record, *Palaeogeogr. Palaeoclimatol. Palaeoecol.*, 142, 123–138, 1998a.

Price, G. D., B. W. Sellwood, R. M. Corfield, L. Clarke, and J. E. Cartlidge, Isotopic evidence for palaeotemperatures and depth stratification of Middle Cretaceous planktonic foraminifera from the Pacific Ocean, *Geol. Mag.*, 135, 183–191, 1998b.

PSUCLIM, Storm activity in ancient climates, 1, Sensitivity of severe storms to climate forcing factors on geologic timescales, *J. Geophys. Res.*, 104, 27,277–27,293, 1999a.

PSUCLIM, Storm activity in ancient climates, 2, An analysis using climate simulations and sedimentary structures, *J. Geophys. Res.*, 104, 27,295–27,320, 1999b.

Ramanathan, V., M. S. Lian, and R. D. Cess, Increased atmospheric CO_2: Zonal and seasonal estimates of the effect on the radiation energy balance and surface temperature, *J. Geophys. Res.*, 84, 4949–4958, 1979.

Retallack, G. J., A 300-million-year record of atmospheric carbon dioxide from fossil plant cuticles, *Nature*, 411, 287–290, 2001.

Rind, D., Relating paleoclimate data and past temperature gradients: Some suggestive rules, *Quat. Sci. Rev.*, 19, 381–390, 2000.

Royer, D. L., R. A. Berner, and D. J. Beerling, Phanerozoic atmospheric CO_2 change: Evaluating geochemical and paleobiological approaches, *Earth Sci. Rev.*, 54, 349–392, 2001.

Schrag, D. P., Effects of diagenesis on the isotopic record of late Paleogene tropical sea surface temperatures, *Chem. Geol.*, 161, 215–224, 1999.

Schrag, D. P., D. J. DePaolo, and F. M. Richter, Reconstructing past sea surface temperatures: Correcting for diagenesis of bulk marine carbonate, *Geochim. Cosmochim. Acta*, 59, 2265–2278, 1995.

Scotese, C. R., and J. Golonka, *ALEOMAP Paleogeographic Atlas*, PALEOMAP Prog. Rep. 20, 43 pp., Dept. of Geol., Univ. of Texas at Arlington, Arlington, Tex., 1992.

Sellwood, B. W., G. D. Price, and P. J. Valdes, Cooler estimates of Cretaceous temperatures, *Nature*, 370, 453–455, 1994.

Shackleton, N. J., and J. P. Kennett, Paleotemperature history of the Cenozoic and the initiation of Antarctic glaciation: Oxygen and carbon isotope analyses in DSDP Sites 277, 279, and 281, *DSDP Init. Rep.*, 29, 743–755, 1975.

Sloan, L. C., and D. Pollard, Polar stratospheric clouds: A high latitude warming mechanism in the ancient greenhouse world, *Geophys. Res. Lett.*, 25, 3517–3520, 1998.

Sloan, L. C., J. C. G. Walker, and T. C. Moore, Possible role of ocean heat transport in early Eocene climate, *Paleoceanography*, 10, 347–356, 1995.

Spero, H. J., J. Bijma, D. W. Lea, and B. E. Bemis, Effect of seawater carbonate concentration on foraminiferal carbon and oxygen isotopes, *Nature*, 390, 497–500, 1997.

Spicer, R. A., and J. T. Parrish, Paleobotanical evidence for cool north polar climates in middle Cretaceous (Albian–Cenomanian) time, *Geology*, 14, 703–706, 1986.

Spicer, R. A., and J. T. Parrish, Late Cretaceous– early Tertiary palaeoclimates of northern high latitudes: A quantitative view, *J. Geol. Soc. London*, 147, 329–341, 1990.

Stoll, H. M., and D. P. Schrag, High-resolution stable isotope records from the Upper Cretaceous rocks of Italy and Spain: Glacial episodes in a greenhouse planet?, *GSA Bull.*, 112, 308–319, 2000.

Tarduno, J. A., D. B. Brinkman, P. R. Renne, R. D. Cottrell, H. Scher, and P. Castillo, Evidence for extreme climatic warmth from Late Cretaceous Arctic Vertebrates, *Science*, 282, 2241–2244, 1998.

Thompson, S. L., and D. Pollard, Greenland and Antarctic mass balances for present and doubled CO_2 from the GENESIS version 2 global climate model, *J. Clim.*, 10, 871–900, 1997.

Trenberth, K. E., and J. M. Caron, The atmospheric energy budget and implications for surface fluxes and ocean heat transports, *Clim. Dyn.*, 17, 259–276, 2001.

van Breugel, Y., S. Schouten, E. Erba, and J. S. Sinninghe Damste, Biogeochemistry of the Aptian Selli event: Examination of the negative isotope spike, Spring 2002 ACS National Meeting Geochemistry Division Technical Program and Abstracts, Am. Chem. Soc. [Online], 2002. (Available as http://membership.acs.org/g/geoc/spring2002abstracts.pdf).

Veizer, J., Y. Godderis, and L. M. Francois, Evidence for decoupling of atmospheric CO_2 and global climate during the Phanerozoic eon, *Nature*, 408, 698–701, 2000.

Wallmann, K., Controls on Cretaceous and Cenozoic evolution of seawater composition, atmospheric CO_2 and climate, *Geochim. Cosmochim. Acta*, 65, 3005–3025, 2001a.

Wallmann, K., The geological water cycle and the evolution of marine $\delta^{18}O$ values, *Geochim. Cosmochim. Acta*, 65, 2469–2485, 2001b.

Weaver, A. J., and E. S. Sarachik, The role of mixed boundary conditions in numerical models of the ocean's climate, *J. Phys. Oceanogr.*, 21, 1470–1493, 1991.

Wilson, P. A., and R. D. Norris, Warm tropical ocean surface and global anoxia during the mid- Cretaceous period, *Nature*, 412, 425–429, 2001.

Wilson, P. A., R. D. Norris, and M. J. Cooper, Testing the Cretaceous greenhouse hypothesis using glassy foraminiferal calcite from the core of the Turonian tropics on Demerara Rise, *Geology*, *30*, 607–610, 2002.

Woo, K. S., T. F. Anderson, L. B. Railsback, and P. A. Sandberg, Oxygen isotope evidence for high-salinity surface seawater in the mid-Cretaceous Gulf of Mexico: Implications for warm, saline deepwater formation, *Paleoceanography*, *7*, 673–685, 1992.

Yapp, C. J., and H. Poths, Carbon isotopes in continental weathering environments and variations in ancient atmospheric CO$_2$ pressure, *Earth Planet. Sci. Lett.*, *137*, 71–82, 1996.

Zachos, J. C., L. D. Stott, and K. C. Lohmann, Evolution of early Cenozoic marine temperatures, *Paleoceanography*, *9*, 353–387, 1994.

Zeebe, R. E., Seawater pH and isotopic paleo-temperatures of Cretaceous oceans, *Palaeogeogr. Palaeoclimatol. Palaeoecol.*, *170*, 49–57, 2001.

Ziegler, A. M., Phytogeographic patterns and continental configurations during the Permian period, in *Palaeozoic, Palaeogeography and Biogeography*, edited by W. S. McKerrow and C. R. Scotese, *Mem. Geol. Soc. Am.*, *12*, 363–379, 1990.

———————————

K. L. Bice, Department of Geology and Geophysics, Woods Hole Oceanographic Institution, Mail Stop 23, Woods Hole, MA 02543, USA. (kbice@whoi.edu)

R. D. Norris, Scripps Institution of Oceanography, University of California, San Diego, 308 Vaughn Hall, La Jolla, CA 92093-0244, USA. (rnorris@ucsd.edu)